National Library of Canada
Bibliothèque nationale du Canada

Canadian Theses Service
Service des thèses canadiennes

Ottawa, Canada
K1A 0N4

NOTICE

The quality of this microform is heavily dependent upon the quality of the original thesis submitted for microfilming. Every effort has been made to ensure the highest quality of reproduction possible.

If pages are missing, contact the university which granted the degree.

Some pages may have indistinct print especially if the original pages were typed with a poor typewriter ribbon or if the university sent us an inferior photocopy.

Previously copyrighted materials (journal articles, published tests, etc.) are not filmed.

Reproduction in full or in part of this microform is governed by the Canadian Copyright Act, R.S.C. 1970, c. C-30.

AVIS

La qualité de cette microforme dépend grandement de la qualité de la thèse soumise au microfilmage. Nous avons tout fait pour assurer une qualité supérieure de reproduction.

S'il manque des pages, veuillez communiquer avec l'université qui a conféré le grade.

La qualité d'impression de certaines pages peut laisser à désirer, surtout si les pages originales ont été dactylographiées à l'aide d'un ruban usé ou si l'université nous a fait parvenir une photocopie de qualité inférieure.

Les documents qui font déjà l'objet d'un droit d'auteur (articles de revue, tests publiés, etc.) ne sont pas microfilmés.

La reproduction, même partielle, de cette microforme est soumise à la Loi canadienne sur le droit d'auteur, SRC 1970, c. C-30.

NL-339 (r. 88/04)

Canada

THE UNIVERSITY OF ALBERTA

IMPEDANCE CALCULATIONS FOR ARTERIAL MODELS

by

© Rong Zhu Gan

A THESIS SUBMITTED TO

THE FACULTY OF GRADUATE STUDIES AND RESEARCH

IN PARTIAL FULFILLMENT OF THE REQUIREMENTS

FOR THE DEGREE OF

MASTER OF SCIENCE

IN

APPLIED MATHEMATICS

DEPARTMENT OF MATHEMATICS

EDMONTON, ALBERTA

FALL, 1988

Permission has been granted to the National Library of Canada to microfilm this thesis and to lend or sell copies of the film.

The author (copyright owner) has reserved other publication rights, and neither the thesis nor extensive extracts from it may be printed or otherwise reproduced without his/her written permission.

L'autorisation a été accordée à la Bibliothèque nationale du Canada de microfilmer cette thèse et de prêter ou de vendre des exemplaires du film.

L'auteur (titulaire du droit d'auteur) se réserve les autres droits de publication; ni la thèse ni de longs extraits de celle-ci ne doivent être imprimés ou autrement reproduits sans son autorisation écrite.

ISBN 0-315-45637-X

THE UNIVERSITY OF ALBERTA

RELEASE FORM

NAME OF AUTHOR: Rong Zhu Gan

TITLE OF THESIS: IMPEDANCE CALCULATIONS FOR ARTERIAL MODELS

DEGREE FOR WHICH THESIS WAS PRESENTED: MASTER OF SCIENCE

YEAR THIS DEGREE GRANTED 1988

Permission is hereby granted to THE UNIVERSITY OF ALBERTA LIBRARY to reproduce single copies of the thesis and to lend or sell such copies for private, scholarly or scientific research purposes only.

The author reserves other publication rights, and neither the thesis nor extensive extracts from it may be printed or otherwise reproduced without the author's written permission.

Gan Rongzhu

SIGNED

PERMANENT ADDRESS:

Department of Mathematics

University of Alberta

Edmonton, Alberta, Canada T6G 2G1

Date July 22, 1988

THE UNIVERSITY OF ALBERTA

THE FACULTY OF GRADUATE STUDIES AND RESEARCH

The undersigned certify that they have read, and recommend to the Faculty of Graduate Studies and Research, for acceptance, a thesis entitled Impedance Calculations for Arterial Models submitted by Rong Zhu Gan in partial fulfilment of the requirements for the degree of Master of Science.

Bryant Moodie

Supervisor

K J Dait

J B Hawthorne

Date July 7, 1988

ABSTRACT

The characteristic and effective impedances for an experimentally tested shell theory model of an arterial pathway with branching are calculated. The influence of viscoelasticity, fluid viscosity, and geometry on these quantities is examined in detail for a broad range of frequencies. Following this, we compute the input impedance for an assembly of branching fluid filled distensible tubes having discrete reflection sites for pressure and/or flow waves. The effects of architecture, viscoelasticity and fluid viscosity are investigated over a natural frequency range occuring in the cardiac output of experimental animals. All the numerical results are depicted graphically and comparisons with *in vivo* measurements are made.

ACKNOWLEDGEMENTS

I wish to express my heart-felt thanks to my supervisor, Professor T.B. Moodie for introducing me to the subject of wave propagation and mathematical haemodynamics and then for investigating a considerable amount of time and effort guiding my research. His help, encouragement and patience were all invaluable.

I would also like to thank Dr. R. Sawatzky for his critical insight through thoughful discussions and Dr. G. Swaters for the much appreciated supervision of my program of study.

Finally my thanks go to Christine Fischer for her excellent typing in preparing the final manuscript.

I am grateful for financial support from Professor Moodie and from the University of Alberta.

TABLE OF CONTENTS

Chapter	Page
Abstract	iv
Acknowledgement	v
List of Figures	vii
I Introduction	1
II The Model	5
III Analysis of an N-furcation	12
$< A >$ Calculation	12
$< B >$ Analysis of Results	21
IV Analysis of an Assembly of Tubes	39
$< A >$ Calculation	39
$< B >$ Analysis of Results	43
V Conclusions	56
Bibliography	57

LIST OF FIGURES

Figure — Page

3.1 Illustrating a trifurcation — 13

3.2 Variation of $|Z^{(1)}|$ with ω for $R^{(1)} = 0.4\text{cm}$, $\tau^{(1)} = 0.15$, and $m^{(1)} = 1666$ (—) , 8791 (- - - -) , 33088 (-·-·-·). — 22

3.3 Variation of $\phi_{Z^{(1)}}$ with ω for $R^{(1)} = 0.4\text{cm}$, $\tau^{(1)} = 0.15$, and $m^{(1)} = 1666$ (—) , 8791 (- - - -) , 33088 (-·-·-·). — 23

3.4 Variation of $|Z^{(1)}|$ with ω for $R^{(1)} = 0.4\text{cm}$, $\tau^{(1)} = 0.05$, and $m^{(1)} = 1666$ (—) , 8791 (- - - -) , 33088 (-·-·-·). — 24

3.5 Variation of $\phi_{Z^{(1)}}$ with ω for $R^{(1)} = 0.4\text{cm}$, $\tau^{(1)} = 0.05$, and $m^{(1)} = 1666$ (—) , 8791 (- - - -) , 33088 (-·-·-·). — 25

3.6 Variation of $|\lambda_c|$ with ω for $R^{(n)}/R^{(1)} = 1/2$, $c_0^{(1)}/c_0^{(n)} = 1$, $\eta^{(1)} = 0.173125$, $\tau^{(1)} = 0.15$, $N = 4$, and $m^{(1)} = 1666$ (—) , 8791 (- - - -) , 33088 (-·-·-·). — 27

3.7 Variation of $|\lambda_c|$ with ω for $R^{(n)}/R^{(1)} = 1$, $c_0^{(1)}/c_0^{(n)} = 2$, $\eta^{(1)} = 0.173125$, $\tau^{(1)} = 0.15$, $N = 4$, and $m^{(1)} = 1666$ (—) , 8791 (- - - -) , 33088 (-·-·-·). — 28

3.8 Variation of $|Z_{\text{eff}}^{(1)}|$ with ω for $R^{(n)}/R^{(1)} = 1/2$, $c_0^{(1)}/c_0^{(n)} = 1$, $\eta^{(1)} = 0.173125$, $\tau^{(1)} = 0.15$, $N = 4$, $\ell = 42\text{cm}$, and $m^{(1)} = 1666$ (—) , 8791 (- - - -) , 33088 (-·-·-·). — 30

Figure Page

3.9 Variation of $\phi_{\text{eff}}^{(1)}$ with ω for $R^{(n)}/R^{(1)} = 1/2$, $c_0^{(1)}/c_0^{(n)} = 1$, $\eta^{(1)} = 0.173125$, $\tau^{(1)} = 0.15$, $N = 4$, $\ell = 42$cm, and $m^{(1)} = 1666$ (—) , 8791 (- - - -) , 33088 (·····). 31

3.10 Variation of $|Z_{\text{eff}}^{(1)}|$ with ω for $R^{(n)}/R^{(1)} = 1/2$, $c_0^{(1)}/c_0^{(n)} = 1$, $\eta^{(1)} = 0.173125$, $\tau^{(1)} = 0.15$, $N = 4$, $m^{(1)} = 8791$, and $\ell = 42$cm (—) , 21cm (- - - -) , 5cm (·····). 32

3.11 Variation of $\phi_{\text{eff}}^{(1)}$ with ω for $R^{(n)}/R^{(1)} = 1/2$, $c_0^{(1)}/c_0^{(n)} = 1$, $\eta^{(1)} = 0.173125$, $\tau^{(1)} = 0.15$, $N = 4$, $m^{(1)} = 8791$, and $\ell = 42$cm (—) , 21cm (- - - -) , 5cm (·····). 33

3.12 Variation of $|Z_{\text{eff}}^{(1)}|$ with ω for $R^{(n)}/R^{(1)} = 1$, $c_0^{(1)}/c_0^{(n)} = 2$, $\eta^{(1)} = 0.173125$, $\tau^{(1)} = 0.15$, $N = 4$, $\ell = 42$cm, and $m^{(1)} = 1666$ (—) 8791 (- - - -) , 33088 (·····). 34

3.13 Variation of $\phi_{\text{eff}}^{(1)}$ with ω for $R^{(n)}/R^{(1)} = 1$, $c_0^{(1)}/c_0^{(n)} = 2$, $\eta^{(1)} = 0.173125$, $\tau^{(1)} = 0.15$, $N = 4$, $\ell = 42$cm, and $m^{(1)} = 1666$ (—) 8791 (- - - -) , 33088 (·····). 35

3.14 Variation of $|Z_{\text{eff}}^{(1)}|$ with ω for $R^{(n)}/R^{(1)} = 1$, $c_0^{(1)}/c_0^{(n)} = 2$, $\eta^{(1)} = 0.173125$, $\tau^{(1)} = 0.15$, $N = 4$, $m^{(1)} = 8791$, and $\ell = 42$cm (—) , 21cm (- - - -) , 5cm (·····). 36

3.15 Variation of $\phi_{\text{eff}}^{(1)}$ with ω for $R^{(n)}/R^{(1)} = 1$, $c_0^{(1)}/c_0^{(n)} = 2$, $\eta^{(1)} = 0.173125$, $\tau^{(1)} = 0.15$, $N = 4$, $m^{(1)} = 8791$, and $\ell = 42$cm (—) , 21cm (- - - -) , 5cm (·····). 37

Figure Page

4.1 Tube assembly for calculating impedance. 40

4.2 Variation of $|Z_{in}|$ with ω for $\tau^{(1)} = 0.15$, $\ell_0 = 10$cm, $\ell_1 = 120$cm, $\ell_2 = 40$cm, $N_1 = N_2 = 3$, $m^{(1)} = 8791$ (—) , 33088 (- - - -) . 44

4.3 Variation of ϕ_Z with ω for $\tau^{(1)} = 0.15$, $\ell_0 = 10$cm, $\ell_1 = 120$cm, $\ell_2 = 40$cm, $N_1 = N_2 = 3$, $m^{(1)} = 8791$ (—) , 33088 (- - - -) . 45

4.4 Variation of $|Z_{in}|$ with ω for $\tau^{(1)} = 0.15$, $\ell_0 = 10$cm, $\ell_1 = 120$cm, $\ell_2 = 40$cm, $N_1 = N_2 = 5$, $m^{(1)} = 8791$ (—) , 33088 (- - - -) . 46

4.5 Variation of ϕ_Z with ω for $\tau^{(1)} = 0.15$, $\ell_0 = 10$cm, $\ell_1 = 120$cm, $\ell_2 = 40$cm, $N_1 = N_2 = 5$, $m^{(1)} = 8791$ (—) , 33088 (- - - -) . 47

4.6 Variation of $|Z_{in}|$ with ω for $\tau^{(1)} = 0.15$, $\ell_0 = 10$cm, $\ell_1 = 80$cm, $\ell_2 = 40$cm, $N_1 = N_2 = 3$, $m^{(1)} = 8791$ (—) , 33088 (- - - -) . 50

4.7 Variation of ϕ_Z with ω for $\tau^{(1)} = 0.15$, $\ell_0 = 10$cm, $\ell_1 = 80$cm, $\ell_2 = 40$cm, $N_1 = N_2 = 3$, $m^{(1)} = 8791$ (—) , 33088 (- - - -) . 51

4.8 Variation of $|Z_{in}|$ with ω for $\tau^{(1)} = 0.15$, $\ell_0 = 20$cm, $\ell_1 = 120$cm, $\ell_2 = 40$cm, $N_1 = N_2 = 3$, $m^{(1)} = 8791$ (—) , 33088 (- - - -) . 52

4.9 Variation of ϕ_Z with ω for $\tau^{(1)} = 0.15$, $\ell_0 = 20$cm, $\ell_1 = 120$cm, $\ell_2 = 40$cm, $N_1 = N_2 = 3$, $m^{(1)} = 8791$ (—) , 33088 (- - - -) . 53

Figure Page

4.10 Variation of $|Z_{in}|$ with ω for $\ell_0 : \ell_2 : \ell_1 = 3 : 14 : 42$ (—), $6 : 24 : 72$ (- - - -), $8 : 30 : 90$ (-·-·-·). 54

4.11 Variation of ϕ_Z with ω for $\ell_0 : \ell_2 : \ell_1 = 3{:}14 : 42$ (—), $6 : 24 : 72$ (- - - -), $8 : 30 : 90$ (-·-·-·). 55

CHAPTER I

Introduction

Pulsatile blood flow is generated in the arteries by the pumping action of the heart and the interaction of blood with the arterial walls. The theory of pulse wave propagation in arteries is a special case of the general theory of one-dimensional waves in fluids. That means the character of the wave propagation is determined by the balance between the resisting force and the inertia of the fluid.

Pulses propagating from the heart to the periphery consist of forward directed waves and backward travelling reflected waves, whose particular features have been recognized to depend on geometrical and physical aspects of the circulatory system. The distensibility of the wall, the lumen area, the viscous effects of the blood and tube wall, and arterial branchings are the major elements affecting wave propagation in arteries.

In a series of recent papers ([1]-[4]), the propagation and reflection of a transient pressure impulse in a viscoelastic tube was investigated experimentally using both water-filled latex rubber tubing and the aorta of anaesthetised dogs. In the experiments reported in these articles, a single pulse of very short duration, roughly 5 ms, was generated in the system, making it possible to observe the incident pulse in isolation from its reflections. The frequency spectrum of such impulses is much broader than that of the natural arterial pulse in humans or dogs: the artificially generated pulses contain frequencies in the range 0-250 Hz

whereas the frequency content of the natural pulse is limited to the range 1-10 Hz in humans and 2-20 Hz in dogs.

Mathematical models of wave propagation can contribute to the quantitative analysis of the arterial wall's mechanical properties, the effect of chemical agents on the vasculature, the detection of pathological alterations (like stenoses or aneurysms) in blood vessels and the study of the role and working of the cardiovascular system's regulatory mechanisms. For this purpose, the availability of an accurate mathematical description of pulse wave transmission in arteries represents a useful support to investigate large portions of the arterial tree, as often required by both clinical practice and physiological investigation.

The usual mathematical analyses of wave propagation in the cardiovascular system are based on a linear long wavelength (LLW) theory [5]. (LLW theory was first introduced by Young [6]. Lighthill [7], [8] and others improved and extended this theory to apply in a variety of situations representive of the cardiovascular system.) The wavelengths of the frequency components present in a given pulse are assumed to be much greater than the radius of the tube involved. In the case of the natural arterial pulse, this assumption is a reasonable one. This theory, however, usually fails to model adequately the transmission characteristics of the pulse in the experiments cited above. In these experiments the lengths of the shorter waves in the impulses are of the same order of magnitude as the radii of the tubes.

A model of pressure pulse propagation in liquid-filled distensible tubes that has a range of validity beyond that of the LLW theory was presented recently by Moodie et. al. [9]. This model is based on a linear medium wavelength (LMW) theory and includes not only the effects of the circumferential stiffness of the tube wall and the axial inertia of the fluid but also the radial inertia of the tube wall and the radial inertia of the fluid. Experiments conducted to test the model demonstrate that it is successful in predicting the transmission characteristics observed in a pressure impulse generated at the entrance of a very long water-filled latex rubber tube [9]. Employing this model, Sawatzky and Moodie [10] explored the reflection characteristics of waves at a junction between two mechanically dissimilar tubes. They noted that the LMW theory, unlike the LLW theory, predicts such reflection to be frequency dependent, although the variation with frequency of the reflections is not large enough to be observed in experiments until frequencies in excess of 100 Hz are reached. In subsequent investigations, Sawatzky and Moodie [11], [12], examined the role of fluid viscosity in the propagation of pressure impulses of the sort generated in the experiments of [1]-[4] and derived formulae for the reflection coefficients at a junction between two dissimilar tubes. Their work confirmed that the dominant dissipative mechanism involved in the propagation of such pulses is that of wall viscoelasticity; but fluid viscosity causes a modest reduction in the peak amplitude of the pressure pulse and this attenuation is very sensitive to the degree of viscosity.

The concepts of characteristic and effective impedance have proved useful in vascular studies ([5],[8],[13],[14],[15],[16]). The characteristic impedance of a uniform fluid-filled tube is defined as the ratio of oscillatory pressure to flow rate in a tube when a single wave is travelling along it and takes the same constant value at every point of the tube. In the presence of wave reflections the measured ratio of oscillatory pressure to flow rate is then called the effective impedance. As such, effective impedance values provide a measure of the resistance to pulsatile flow of a given system and, in the case of the functioning cardiovascular system, provide a measure of the work performed by the heart in driving such flows. Effective impedance is also called input impedance of the system distal to the sight of measurement [14], [15].

In this thesis, we shall incorporate the experimentally tested LMW model ([9], [11]) for impulse propagation in a tube into definitions of both the characteristic and effective impedance in order to examine their dependence upon the various parameters of the system over a wide range of frequencies. Furthermore, the input impedance of a system of branching tubes with multiple reflection sites is investigated over the physiological frequency range. This input impedance will then be evaluated as a function of frequency and discussed in the light of certain physiological observations.

CHAPTER II

The Model

As a consequence of the analysis and the subsequent experimental confirmation carried out in [9], we take as the equation of motion for the incompressible "tethered" tube wall

$$4G_e(1+\tau\frac{\partial}{\partial t})\frac{h}{R^2}W = P - \gamma h\frac{\partial^2 W}{\partial t^2}, \tag{2.1}$$

where W is the radial displacement of the tube wall, G_e is the equlibrium shear modulus, t the time, R the tube radius, h the wall thickness, γ the density of the wall, τ the retardation time for the wall material, ρ the density of the fluid, and P the net radial stress across the tube wall directed outwardly, which is defined as

$$P = \sigma_i - \sigma_e, \tag{2.2}$$

here σ_i is the normal stress inside the tube, called the internal fluid stress, σ_e is the stress acting on the outside of the tube, called the external pressure load. We assume that p_e is constant and equal to the undisturbed fluid pressure within the tube, that is, $p_e = 0$.

The fluid equations are the linearized Navier-Stokes equations, together with the continuity equation. Their axisymmetric forms are

$$\frac{\partial v_r}{\partial t} = -\frac{1}{\rho}\frac{\partial p}{\partial r} + \nu\Big[\frac{\partial^2 v_r}{\partial r^2} + \frac{1}{r}\frac{\partial v_r}{\partial r} - \frac{v_r}{r^2} + \frac{\partial^2 v_r}{\partial x^2}\Big], \tag{2.3}$$

$$\frac{\partial v_x}{\partial t} = -\frac{1}{\rho}\frac{\partial p}{\partial x} + \nu\Big[\frac{\partial^2 v_x}{\partial r^2} + \frac{1}{r}\frac{\partial v_x}{\partial r} + \frac{\partial^2 v_x}{\partial x^2}\Big], \tag{2.4}$$

$$\frac{\partial v_x}{\partial x} + \frac{\partial v_r}{\partial r} + \frac{v_r}{r} = 0, \tag{2.5}$$

where v_r is the radial fluid velocity, v_x the axial fluid velocity, p the fluid pressure and $p(R,x,t) = p_i$, r the radial coordinate measured from the axis of the tube, x the axial coordinate, and ν the kinematic viscosity of the fluid.

At the interface between the fluid and the solid, the conditions are the continuity of radial and axial components of velocity and the continuity of pressure:

$$v_r(R,x,t) = \frac{\partial W(x,t)}{\partial t}, \tag{2.6}$$

$$v_x(R,x,t) = 0, \tag{2.7}$$

$$\begin{aligned} P(x,t) &= [p - 2\nu\rho\frac{\partial v_r}{\partial r}]_{r=R} - p_e(x,t) \\ &= [p - 2\nu\rho\frac{\partial v_r}{\partial r}]_{r=R}. \end{aligned} \tag{2.8}$$

The fluid and tube wall are to be set in motion by a rise in pressure at $x = 0$. It is convenient to prescribe the disturbance at $x = 0$ in terms of p_m, the fluid pressure averaged over the tube's cross section, and to express the solution in terms of p_m and v_m (the axial fluid velocity averaged over a cross section). These quantities are then given by

$$p_m(x,t) = \frac{1}{A}\int_A\int p(r,x,t)dA, \tag{2.9}$$

$$v_m(x,t) = \frac{1}{A}\int_A\int v_x(r,x,t)dA, \tag{2.10}$$

where A is the area of the tube's cross section.

It is convenient to express the problem in nondimensional variables. To this end, we introduce the following dimensionless quantities:

$$\left.\begin{aligned}(\hat{x},\hat{r},\widehat{W}) = (x,r,W)/R, (\hat{t},\hat{\tau}) = (t,\tau)\frac{c_0}{R},\\ (\hat{v}_x,\hat{v}_r,\hat{v}_m) = (v_x,v_r,v_m)/c_0, (\hat{p},\hat{P},\hat{p}_m) = (p,P,p_m)/\rho c_0^2.\end{aligned}\right\} \tag{2.11}$$

In the sequel the following nondimensional quantities appear as well:

$$\hat{k} = kR, \quad \hat{\omega} = \omega R/c_0, \tag{2.12}$$

and

$$\eta = \frac{1}{8} + \frac{\gamma h}{2\rho R}, \quad m = c_0 R/\nu, \tag{2.13}$$

wherein hats are employed to denote nondimensional quantities, c_0 is the Korteweg-Moens wave speed for a "tethered", incompressible, viscoelastic, thin-walled circular cylinder, that is,

$$c_0 = \left(\frac{2G_e h}{pR}\right)^{\frac{1}{2}}, \tag{2.14}$$

k and ω are the wave number and circular frequency for a wave component and m is a Reynolds number. In the the absence of a natural velocity scale arising from the flow, the typical velocity used in the formula for m is the one associated with the pressure disturbance.

After substitution of the appropriate nondimensional quantities from the above equations into the wall equation (2.1) and the fluid equations (2.3)-(2.5), the following nondimensional governing equations are obtained

$$2(\tau\frac{\partial}{\partial t} + 1)W = P - \frac{\gamma h}{\rho R}\frac{\partial^2 W}{\partial t^2}, \tag{2.15}$$

$$\frac{\partial v_r}{\partial t} = -\frac{\partial p}{\partial r} + \frac{\nu}{c_0 R}\left[\frac{\partial^2 v_r}{\partial r^2} + \frac{1}{r}\frac{\partial v_r}{\partial r} - \frac{v_r}{r^2} + \frac{\partial^2 v_r}{\partial x^2}\right], \tag{2.16}$$

$$\frac{\partial v_z}{\partial t} = -\frac{\partial p}{\partial x} + \frac{\nu}{c_0 R}\left[\frac{\partial^2 v_z}{\partial r^2} + \frac{1}{r}\frac{\partial v_z}{\partial r} + \frac{\partial^2 v_z}{\partial x^2}\right], \tag{2.17}$$

$$\frac{\partial v_z}{\partial x} + \frac{\partial v_r}{\partial r} + \frac{v_r}{r} = 0, \tag{2.18}$$

or

$$2(\tau\frac{\partial}{\partial t} + 1)W = P - 2(\eta - \frac{1}{8})\frac{\partial^2 W}{\partial t^2}, \tag{2.19}$$

$$\frac{\partial v_r}{\partial t} = -\frac{\partial p}{\partial r} + \frac{1}{m}\left[\frac{\partial^2 v_r}{\partial r} + \frac{1}{r}\frac{\partial v_r}{\partial r} - \frac{v_r}{r^2} + \frac{\partial^2 v_r}{\partial x^2}\right], \tag{2.20}$$

$$\frac{\partial v_z}{\partial t} = -\frac{\partial p}{\partial x} + \frac{1}{m}\left[\frac{\partial^2 v_z}{\partial r^2} + \frac{1}{r}\frac{\partial v_z}{\partial r} + \frac{\partial^2 v_z}{\partial x^2}\right], \tag{2.21}$$

$$\frac{\partial v_z}{\partial x} + \frac{\partial v_r}{\partial r} + \frac{v_r}{r} = 0, \tag{2.22}$$

where the hats have been dropped from the nondimensional variables for convenience, and will be dropped in the succeeding equations as well.

The interface conditions Eqs. (2.6)-(2.8) become

$$v_r(1, x, t) = \frac{\partial W(x,t)}{\partial t}, \tag{2.23}$$

$$v_z(1, x, t) = 0, \tag{2.24}$$

$$P(x,t) = \left[p - \frac{2}{m}\frac{\partial v_r}{\partial r}\right]_{r=1}. \tag{2.25}$$

The mean fluid pressure and the averaged axial velocity are then given by

$$p_m(x,t) = 2\int_0^1 r p(r,x,t)dr, \tag{2.26}$$

$$v_m(x,t) = 2\int_0^1 r v_z(r,x,t)dr, \tag{2.27}$$

Since the model includes dissipative mechanisms, the dispersive waves are usually recognized by existence of the elementary solutions in the form of

$$\{p, p_m, v_m, v_z, v_r, W\} = \{\bar{p}, \bar{p}_m, \bar{v}_m, \bar{v}_z, \bar{v}_r, \bar{W}\} \exp(ikx - i\omega t), \tag{2.28}$$

where $\bar{p}(r), \bar{p}_m(r), \bar{v}_m(r), \bar{v}_z(r), \bar{v}_r(r), \bar{W}(r)$ are the amplitudes.

Substituting these equations into the governing equations (2.19)-(2.22), the interface conditions (2.23)-(2.25), and Eqs. (2.26)-(2.27), we obtain

$$p_m(x,t) = \frac{2I_1(k)}{k} a_1 \exp(ikx - i\omega t), \tag{2.29}$$

$$v_m(x,t) = \frac{2I_1(k)}{\omega}\left[1 - \frac{F(k)}{F(K)}\right] a_1 \exp(ikx - i\omega t), \tag{2.30}$$

wherein a_1 is an arbitrary constant, F is defined in terms of the modified Bessel functions as

$$F(z) = zI_0(z)/2I_1(z), \tag{2.31}$$

and I_n denotes the modified Bessel function of the first kind of order n, $n = 0, 1$, and K is given as

$$K = (k^2 - im\omega)^{\frac{1}{2}}. \tag{2.32}$$

On the otherhand, after substituting the elementary solutions into the wall equation (2.19), the dispersion relation takes the form

$$k^2\left[\frac{1}{F(k)} - \frac{1}{F(K)}\right]\left[\Lambda(\omega) + \frac{1}{8}\omega^2 + \frac{i\omega}{m}\right] = \omega^2, \tag{2.33}$$

where

$$\Lambda(\omega) = 1 - i\omega\tau - \omega^2\eta \tag{2.34}$$

The approximate solutions for the roots of Eq. (2.33) are given as

$$k = \pm\omega(F_2(K_0)\Lambda)^{-\frac{1}{2}}\left[1+\frac{1}{2}\Big(\frac{F_3(K_0)}{F_2(K_0)\Lambda}-\frac{A_1(K_0)}{(F_2(K_0)\Lambda)^2}\Big)\omega^2\right]+O\Big[\frac{F_3^2(K_0)\omega^4}{F_2^2(K_0)\Lambda^2}\Big], \quad (2.35)$$

wherein

$$K_0 = (m\omega)^{\frac{1}{2}}e^{-i\frac{\pi}{4}}, \quad (2.36)$$

$$A_1(z) = (F_1(z)-\frac{1}{8})/F(z), \quad (2.37)$$

$$F_1(z) = \Big[F(z)(1-F(z))/z^2\Big]+\frac{1}{4}, \quad (2.38)$$

$$F_2(z) = 1-1/F(z), \quad (2.39)$$

$$F_3(z) = \frac{F_1(z)+\frac{1}{8}}{F(z)}-\frac{F_2(z)}{z^2}. \quad (2.40)$$

The approximation is uniformly valid throughout the range of interest in the frequency ω and the kinematic fluid viscosity ν, except at the point $\omega = 0$, $\nu = 0$ where the dependence of k upon ω and ν is nonuniform. The entire frequency range considered here are associated with the dimensionless interval $0 \leq \omega \leq 1.5$.

The general solutions for p_m, u_m can be constructed directly from the above equations by means of Fourier integrals [17]. Since the dispersion relation possesses a pair of roots $\pm k$ given by Eq. (2.35) the Fourier integrals will contain two terms corresponding to each of the two roots. Thus the general solution for p_m is

$$p_m(x,t) = \frac{1}{2\pi}\int_{-\infty}^{\infty}[p^+(\omega)e^{ikx}+p^-(\omega)e^{-ikx}]e^{-i\omega t}\,d\omega, \quad (2.41)$$

and the general solution for v_m is

$$v_m(x,t) = \frac{1}{2\pi}\int_{-\infty}^{\infty}\frac{k}{\omega}\Big[1-\frac{F(k)}{F(K)}\Big][p^+(\omega)e^{ikx}-p^-(\omega)e^{-ikx}]e^{-i\omega t}\,d\omega, \quad (2.42)$$

here p^+ and p^- are chosen to fit the boundary conditions corresponding to $+k(\omega)$ and $-k(\omega)$, respectively.

Suppose that the prescribed disturbance is given by

$$p_m(0,t) = \phi(t), \tag{2.43}$$

where $\phi(t)$ is a function which rises steadily after $t = 0$ from zero to a maximum value of one and then decreases steadily back to zero. Then,

$$p^+(\omega) = \bar{\phi}(\omega), p^-(\omega) = 0, \tag{2.44}$$

where $\bar{\phi}(\omega)$ is the Fourier transform of $\phi(t)$, that is,

$$\bar{\phi}(\omega) = \int_0^\infty \phi(t) e^{i\omega t}\, dt. \tag{2.45}$$

Thus, the solution satisfying all of the prescribed conditions including quiescent initial and regularity conditions imposed as $x \to \infty$ or $t \to \infty$ may be expressed as

$$p_m(x,t) = \frac{1}{2\pi} \int_{-\infty}^{\infty} \bar{\phi}(\omega) \exp[i(kx - \omega t)] d\omega, \tag{2.46}$$

$$v_m(x,t) = \frac{1}{2\pi} \int_{-\infty}^{\infty} \frac{k}{\omega} \bar{\phi}(\omega) \left[1 - \frac{F(k)}{F(K)}\right] \exp[i(kx - \omega t)] d\omega. \tag{2.47}$$

CHAPTER III

Analysis of an N-furcation

The larger systematic arteries, shown in Fig. 2.10 of McDonald [14], conduct the blood from the heart to the peripheral organs and their dimensions are given in Table I of Caro et al. [18]. This figure shows that arteries progressively divide and subdivide in the process of arborization. Except for the aortic arch, the other arteries have an approximately constant diameter between junctions. The total arterial cross-sectional area increases progressively as it branches. This increase is believed to be necessary to offset the loss in pressure due to increased friction consequent upon the expanding initial surface as the arteries dichotomize.

We now show how the preceding experimentally tested theory may be adapted to compute the effective impedance for a configuration of tubes resembling a typical junction found in the mammalian cardiovascular system.

$< A >$ Calculation

Consider a branching system composed of N tubes meeting in the "compact" [8] junction B located at $x = \ell$ as shown in Fig. (3.1). A pressure impulse of the sort used in the experiments of [1]-[4] is generated at $x = 0$ and travels along Tube 1 toward the junction. We enote the parameters associated with the various tubes by $R^{(n)}$, $h^{(n)}$, $\gamma^{(n)}$, $G_e^{(n)}$, $\tau^{(n)}$, $c_0^{(n)}$, $\eta^{(n)}$, and $m^{(n)}$. According to the prescribed model it is natural to define the characteristic impedence $Z^{(n)}$ of Tube n as the ratio of the averaged normal stress in the axial direction to the

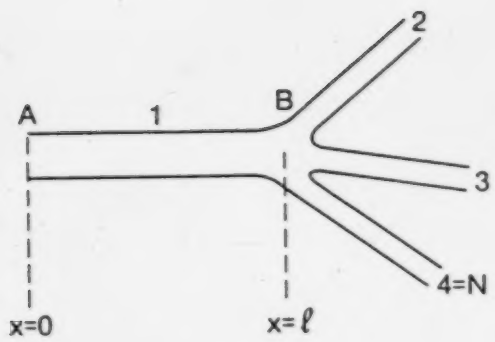

Fig. 3.1 Illustrating a trifurcation

volume flow [19], that is,

$$Z^{(n)} = [p_m^{(n)} - \frac{2}{m^{(n)}} \frac{\partial v_m^{(n)}}{\partial x}] / \pi (R^{(n)})^2 v_m^{(n)}, \quad n = 1, \dots N, \tag{3.1}$$

in dimensionless form, where p_m and v_m were defined in Eqs. (2.26) and (2.27) and given explicitly by Eqs. (2.46)-(2.47). In order to maintain consistency, it is necessary to make all variables nondimensional employing the parameters of one of the tubes. We choose those of Tube 1. It then follows from Eqs. (3.1), (2.46)-(2.47) that

$$\begin{aligned} Z^{(n)} =& \Big\{ 1 - \frac{2i(k^{(n)})^2}{m^{(1)}\omega} \Big[1 - \frac{F(k^{(n)} R^{(n)}/R^{(1)}}{F(K^{(n)})} \Big] \Big\} \\ & \Big\{ \pi \Big(\frac{R^{(n)}}{R^{(1)}} \Big)^2 \frac{k^{(n)}}{\omega} \Big[1 - \frac{F(k^{(n)} R^{(n)}/R^{(1)})}{F(K^{(n)})} \Big] \Big\}^{-1}, \\ & n = 1, \dots, N. \end{aligned} \tag{3.2}$$

where

$$\begin{aligned} k^{(n)} =& \omega \frac{c_0^{(1)}}{c_0^{(n)}} (F_2(K_0^{(n)}) \Lambda^{(n)})^{-\frac{1}{2}} \\ & \Big[1 + \frac{\omega^2}{2} \Big(\frac{F_3(K_0^{(n)})}{F_2(K_0^{(n)}) \Lambda^{(n)}} - \frac{A_1(K_0^{(n)})}{(F_2(K_0^{(n)}) A^{(n)})^2} \Big) \Big(\frac{R^{(n)} c_0^{(1)}}{R^{(1)} c_0^{(n)}} \Big)^2 \Big], \end{aligned} \tag{3.3}$$

$$\Lambda^{(n)} = 1 - i\omega\tau^{(n)} - \omega^2 \Big(\frac{R^{(n)} c_0^{(1)}}{R^{(1)} c_0^{(n)}} \Big)^2 \eta^{(n)}, \tag{3.4}$$

$$K^{(n)} = \Big[(k^{(n)})^2 \Big(\frac{R^{(n)}}{R^{(1)}} \Big)^2 - i m^{(n)} \omega \Big(\frac{R^{(n)} c_0^{(1)}}{R^{(1)} c_0^{(n)}} \Big) \Big]^{\frac{1}{2}}, \tag{3.5}$$

$$K_0^{(n)} = \Big[m^{(n)} \omega \Big(\frac{R^{(n)} c_0^{(1)}}{R^{(1)} c_0^{(n)}} \Big) \Big]^{\frac{1}{2}} e^{-i\frac{\pi}{4}}. \tag{3.6}$$

It is now evident that $Z^{(n)}$ are functions of frequency, wall viscoelasticity, fluid viscosity, and geometric dimensions, but are independent of the position in the tube.

When the pressure or flow pulse arrives at the junction, part of it is reflected back to the parent tube and part transmitted down the daughter tubes $n = 2, 3, \ldots, N$. These incident, reflected,and transmitted pressure waves take the form

$$\begin{aligned} p^i_{m1}(x,t) &= \frac{1}{2\pi}\int_{-\infty}^{\infty} \bar{\phi}(\omega)\exp[i(k^{(1)}x - \omega t)]d\omega \\ &= \frac{1}{2\pi}\int_{-\infty}^{\infty} \hat{p}^i_{m1}(\ell,\omega)\exp[i(k^{(1)}x - \omega t)]d\omega \\ &= \frac{1}{2\pi}\int_{-\infty}^{\infty} \bar{p}^i_{m1}(x,\omega)e^{-i\omega t}\,d\omega, \end{aligned} \tag{3.7}$$

$$\begin{aligned} p^r_{m1}(x,t) &= \frac{1}{2\pi}\int_{-\infty}^{\infty} \bar{a}^r(\omega)\exp[i(-k^{(1)}x - \omega t)]d\omega \\ &= \frac{1}{2\pi}\int_{-\infty}^{\infty} \hat{p}^r_{m1}(\ell,\omega)\exp[i(-k^{(1)}x - \omega t)]d\omega \\ &= \frac{1}{2\pi}\int_{-\infty}^{\infty} \bar{p}^r_{m1}(x,\omega)e^{-i\omega t}\,d\omega, \end{aligned} \tag{3.8}$$

$$\begin{aligned} p^t_{mn}(x,t) &= \frac{1}{2\pi}\int_{-\infty}^{\infty} \bar{a}^r_n(\omega)\exp[i(k^{(n)}x - \omega t)]d\omega \\ &= \frac{1}{2\pi}\int_{-\infty}^{\infty} \hat{p}^t_{m1}(\ell,\omega)\exp[i(k^{(n)}x - \omega t)]d\omega \\ &= \frac{1}{2\pi}\int_{-\infty}^{\infty} \bar{p}^t_{mn}(x,\omega)e^{-i\omega t}\,d\omega, \end{aligned} \tag{3.9}$$

wherein $\bar{\phi}(\omega)$ is determined by the incident waveform and $\bar{a}^r(\omega)$, $\bar{a}^t_n(\omega)$ are determined from the boundary conditions at the junction. Similarly, the incident,

reflected, and transmitted velocity impulses take the form

$$\begin{aligned} v^i_{m1}(x,t) &= \frac{1}{2\pi}\int_{-\infty}^{\infty} \frac{k^{(1)}}{\omega}\bar{\phi}(\omega)\Big[1-\frac{F(k^{(1)})}{F(K^{(1)})}\Big]\exp[i(k^{(1)}x-\omega t)]d\omega \\ &= \frac{1}{2\pi}\int_{-\infty}^{\infty} \hat{v}^i_{m1}(\ell,\omega)\exp[i(k^{(1)}x-\omega t)]d\omega \\ &= \frac{1}{2\pi}\int_{-\infty}^{\infty} \bar{v}^i_{m1}(x,\omega)e^{-i\omega t}\,d\omega, \end{aligned} \tag{3.10}$$

$$\begin{aligned} v^r_{m1}(x,t) &= -\frac{1}{2\pi}\int_{-\infty}^{\infty} \frac{k^{(1)})}{\omega}\bar{a}^r(\omega)\Big[1-\frac{F(k^{(1)})}{F(K^{(1)})}\Big]\exp[i(k^{(1)}x-\omega t)]d\omega \\ &= \frac{1}{2\pi}\int_{-\infty}^{\infty} \hat{v}^r_{m1}(\ell,\omega)\exp[i(-k^{(1)}x-\omega t)]d\omega \\ &= \frac{1}{2\pi}\int_{-\infty}^{\infty} \bar{v}^r_{m1}(x,\omega)e^{-i\omega t}\,d\omega, \end{aligned} \tag{3.11}$$

$$\begin{aligned} v^t_{mn}(x,t) &= \frac{1}{2\pi}\int_{-\infty}^{\infty} \frac{k^{(n)}}{\omega}\bar{a}^t_n(\omega)\Big[1-\frac{F(R^{(n)}k^{(n)}/R^{(1)})}{F(K^{(n)})}\Big]\exp[i(k^{(n)}x-\omega t)]d\omega \\ &= \frac{1}{2\pi}\int_{-\infty}^{\infty} \hat{v}^t_{mn}(\ell,\omega)\exp[i(k^{(n)}x-\omega t)]d\omega \\ &= \frac{1}{2\pi}\int_{-\infty}^{\infty} \bar{v}^t_{mn}(x,\omega)e^{-i\omega t}\,d\omega. \end{aligned} \tag{3.12}$$

The boundary conditions at the junction are derived from the continuity of the averaged normal stress in the axial direction and the volume flow across the junction. These are

$$\begin{aligned} &\bar{p}^i_{m1}(\ell,\omega)-\frac{2ik^{(1)}}{m^{(1)}}\bar{v}^i_{m1}(\ell,\omega)+\bar{p}^r_{m1}(\ell,\omega)+\frac{2ik^{(1)}}{m^{(1)}}\bar{v}^r_{m1}(\ell,\omega) \\ &\qquad = \bar{p}^t_{mn}(\ell,\omega)-\frac{2ik^{(n)}}{m^{(1)}}\bar{v}^t_{mn}(\ell,\omega), \end{aligned} \tag{3.13}$$

and

$$(R^{(1)})^2[\bar{v}^i_{m1}(\ell,\omega)+\bar{v}^r_{m1}(\ell,\omega)] = \sum_{n=2}^{N}(R^{(n)})^2\bar{v}^t_{mn}(\ell,\omega). \tag{3.14}$$

For convenience we introduce the ratio of axial velocity to pressure, that is,

$$\beta = \bar{v}_m(x,\omega)/\bar{p}_m(x,\omega),$$

in the incident, reflected,and transmitted waves. Hence we have the quantities

$$\beta^{(1)} = \frac{\bar{v}^i_{m1}(\ell,\omega)}{\bar{p}^i_{m1}(\ell,\omega)} = -\frac{\bar{v}^r_{m1}(\ell,\omega)}{\bar{p}^r_{m1}(\ell,\omega)} = \frac{k^{(1)}}{\omega}\Big[1 - \frac{F(k^{(1)})}{F(K^{(1)})}\Big], \tag{3.15}$$

$$\beta^{(n)} = \frac{\bar{v}^t_{mn}(\ell,\omega)}{\bar{p}^t_{mn}(\ell,\omega)} = \frac{k^{(n)}}{\omega}\Big[1 - \frac{F(k^{(n)}R^{(n)}/R^{(1)})}{F(K^{(n)})}\Big]. \tag{3.16}$$

Defining the reflection coefficient R_c and the transmission coefficients T_{cn} by

$$R_c = \frac{\bar{p}^r_{m1}(\ell,\omega)}{\bar{p}^i_{m1}(\ell,\omega)}, T_{cn} = \frac{\bar{p}^t_{mn}(\ell,\omega)}{\bar{p}^i_{m1}(\ell,\omega)}, \tag{3.17}$$

we may express Eqs. (3.13) and (3.14) in the form

$$(1+R_c)\Big[1 - \frac{2ik^{(1)}}{m^{(1)}}\beta^{(1)}\Big] = T_{cn}\Big[1 - \frac{2ik^{(n)}}{m^{(1)}}\beta^{(n)}\Big], \tag{3.18}$$

$$\beta^{(1)}(1-R_c) = \sum_{n=2}^{N}(R^{(n)}/R^{(1)})^2\beta^{(n)}T_{cn}. \tag{3.19}$$

The solution of these N equations is

$$R_c = \frac{1-\lambda_c}{1+\lambda_c}, \tag{3.20}$$

$$T_{cn} = \Big[\frac{1 - \frac{2ik^{(1)}}{m^{(1)}}\beta^{(1)}}{1 - \frac{2ik^{(n)}}{m^{(1)}}\beta^{(n)}}\Big]\frac{2}{1+\lambda_c}, \quad n = 2,\dots N, \tag{3.21}$$

where

$$\lambda_c = \lambda_{c2} + \lambda_{c3} + \cdots + \lambda_{cN} = \sum_{n=2}^{N}\lambda_{cn}, \tag{3.22}$$

$$\lambda_{cn} = \Big(\frac{R^{(n)}}{R^{(1)}}\Big)^2\frac{\beta^{(n)}}{\beta^{(1)}}\Big[\frac{1 - \frac{2ik^{(1)}}{m^{(1)}}\beta^{(1)}}{1 - \frac{2ik^{(n)}}{m^{(1)}}\beta^{(n)}}\Big]. \tag{3.23}$$

Here λ_c is the discontinuity coefficient of the junction as the whole whereas λ_{cn} characterizes the discontinuity between the parent and each of the daughter tubes $(n = 2, 3, \ldots, N)$. It is a straightforward matter to show that

$$\lambda_{cn} = Z^{(1)}/Z^{(n)}, \tag{3.24}$$

and

$$\lambda_c = Z^{(1)}/Z_B, \tag{3.25}$$

where

$$(Z_B)^{-1} = (Z^{(2)})^{-1} + (Z^{(3)})^{-1} + \cdots + (Z^{(N)})^{-1}. \tag{3.26}$$

Thus Z_B represents the total impedance of all the daughter tubes lumped together. The reflection coefficient R_c may also be expressed in terms of characteristic impedances, that is,

$$R_c = \frac{1 - Z^{(1)}/Z_B}{1 + Z^{(1)}/Z_B}. \tag{3.27}$$

The above formulae show that the response of a wave to a single junction may be expressed in terms of the characteristic impedances of all tubes meeting at the junction. However, should a reflected wave be present then for that tube carrying such a wave its characteristic impedance must be replaced by its effective impedance in the above formulae.

The rate of energy transfer in the reflected wave relative to that in the incident wave is

$$\frac{E^r}{E^i} = \frac{\pi (R^{(1)})^2 \bar{v}^r_{m1} \left(\bar{p}^r_{m1} - \frac{2}{m^{(1)}} \frac{\partial \bar{v}^r_{m1}}{\partial x}\right)}{\pi (R^{(1)})^2 \bar{v}^i_{m1} \left(\bar{p}^i_{m1} - \frac{2}{m^{(1)}} \frac{\partial \bar{v}^i_{m1}}{\partial x}\right)} = \left(\frac{\bar{p}^r_{m1}}{\bar{p}^i_{m1}}\right)^2 = R_c^2. \tag{3.28}$$

The rate of energy transfer in the transmitted wave to that in the incident wave is

$$\begin{aligned}\frac{E^t}{E^i} &= \frac{\sum_{n=2}^{N} \pi (R^{(n)})^2 \bar{v}^t_{mn} \left(\bar{p}^t_{mn} - \frac{2ik^{(n)}}{m^{(1)}} \bar{v}^t_{mn}\right)}{\pi (R^{(1)})^2 \bar{v}^i_{m1} \left(\bar{p}^i_{m1} - \frac{2}{m^{(1)}} \frac{\partial \bar{v}^i_{m1}}{\partial x}\right)} \\ &= \sum_{n=2}^{N} \left(\frac{R^{(n)}}{R^{(1)}}\right)^2 \frac{\beta^{(n)}}{\beta^{(1)}} \left[\frac{1 - \frac{2ik^{(1)}}{m^{(1)}} \beta^{(1)}}{1 - \frac{2ik^{(n)}}{m^{(1)}} \beta^{(n)}}\right] \frac{4}{(1+\lambda_c)^2} \\ &= \lambda_c \frac{4}{(1+\lambda_c)^2}. \end{aligned} \tag{3.29}$$

Thus, the energy flow equation is

$$\frac{E^r}{E^i} + \frac{E^t}{E^i} = 1, \tag{3.30}$$

or

$$R_c^2 + \sum_{n=2}^{N} \lambda_{cn} \left[\frac{1 - \frac{2ik^{(n)}}{m^{(1)}} \beta^{(n)}}{1 - \frac{2ik^{(1)}}{m^{(1)}} \beta^{(1)}}\right]^2 T_{cn}^2 = 1. \tag{3.31}$$

This shows that no energy is lost at the junction.

The transmission properties of Tube 1, when reflected waves from the junction at $x = \ell$ are present, may be characterized in terms of the effective impedance $Z^{(1)}_{\text{eff}}$, where

$$Z^{(1)}_{\text{eff}}(x, \omega) = \frac{p_{m1} - \frac{2}{m^{(1)}} \frac{\partial v_{m1}}{\partial x}}{\pi (R^{(1)})^2 v_{m1}}, \tag{3.32}$$

with

$$p_{m1} = p^i_{m1}(x,t) + p^r_{m1}(x,t), \tag{3.33}$$

$$v_{m1} = v^i_{m1}(x,t) + v^r_{m1}(x,t). \tag{3.34}$$

It follows from Eqs. (3.7), (3.8), (3.10), (3.11), (3.32)-(3.34) that

$$Z_{\text{eff}}^{(1)}(x,\omega) = \frac{\bar{p}_{m1}^{i}(x,\omega) + \bar{p}_{m1}^{r}(x,\omega) - \frac{2ik^{(1)}}{m^{(1)}}[\bar{v}_{m1}^{i}(x,\omega) - \bar{v}_{m1}^{r}(x,\omega)]}{\pi(R^{(1)})^2[\bar{v}_{m1}^{i}(x,\omega) + \bar{v}_{m1}^{r}(x,\omega)]}. \tag{3.35}$$

Thus, when $x = \ell$,

$$\begin{aligned} Z_{\text{eff}}^{(1)}(\ell,\omega) &= \bar{p}_{m1}^{i}(\ell,\omega)\frac{[1 + R_c - \frac{2ik^{(1)}}{m^{(1)}}(\beta^{(1)} + \beta^{(1)}R_c)]}{\pi(R^{(1)})^2\bar{v}_{m1}^{i}(\ell,\omega)(1 - R_c)} \\ &= \frac{(1 + R_c)[1 - \frac{2ik^{(1)}}{m^{(1)}}\beta^{(1)}]}{(1 - R_c)\pi(R^{(1)})^2\beta^{(1)}}, \end{aligned} \tag{3.36}$$

or

$$Z_{\text{eff}}^{(1)}(\ell,\omega) = Z_B. \tag{3.37}$$

Thus the effective impedance in Tube 1 at the junction is equal to the total impedance presented by the complete network of daughter tubes. When $x = 0$,

$$\begin{aligned} Z_{\text{eff}}^{(1)}(0,\omega) &= \frac{\widehat{p}_{m1}^{i}(\ell,\omega)\left[1 + \frac{\widehat{p}_{m1}^{r}(\ell,\omega)}{\widehat{p}_{m1}^{i}(\ell,\omega)} - \frac{2ik^{(1)}}{m^{(1)}}\left(\frac{\widehat{v}_{m1}^{i}(\ell,\omega)}{\widehat{p}_{m1}^{i}(\ell,\omega)} - \frac{\widehat{v}_{m1}^{r}(\ell,\omega)}{\widehat{p}_{m1}^{i}(\ell,\omega)}\right)\right]}{\pi(R^{(1)})^2\widehat{v}_{m1}^{i}(\ell,\omega)\left[1 + \frac{\widehat{v}_{m1}^{r}(\ell,\omega)}{\widehat{v}_{m1}^{i}(\ell,\omega)}\right]} \\ &= \frac{1 + \bar{R}_c - \frac{2ik^{(1)}}{m^{(1)}}(\beta^{(1)} + \beta^{(1)}\bar{R}_c)}{\pi(R^{(1)})^2\beta^{(1)}(1 - \bar{R}_c)} \\ &= \left(\frac{1 + \bar{R}_c}{1 - \bar{R}_c}\right)Z^{(1)}, \end{aligned} \tag{3.38}$$

where

$$\bar{R}_c = \frac{\widehat{p}_{m1}^{r}(\ell,\omega)}{\widehat{p}_{m1}^{i}(\ell,\omega)} = R_c e^{2ik^{(1)}\ell}. \tag{3.39}$$

Thus we may write

$$Z_{\text{eff}}^{(1)}(0,\omega) = \left[\frac{1 - i\lambda_c \tan(k^{(1)}\ell)}{\lambda_c - i\tan(k^{(1)}\ell)}\right]^2 Z^{(1)}. \tag{3.40}$$

This formula for the effective impdance shows clearly its dependence upon the distance to the reflection site, the frequency, and the mechanical and geometrical parameters of the system. These dependences will be explored in the following section.

$< B >$ Analysis of Results

The characteristic impedance $Z^{(1)}$ or $Z^{(n)}$ presented in Eq. (3.2) are functions of frequency and their frequency dependence varies with the parameters m and τ. The dependence of the modulus, $|Z^{(1)}|$, and the phase angle, $\phi_{Z^{(1)}}$, of $Z^{(1)}$ on the dimensionless frequency ω is displayed in Figs. (3.2)-(3.5). Here we have chosen $R^{(1)} = 0.4cm$, $c_0^{(1)} = 833cm/s$, and $\eta^{(1)} = 0.173125$. Thus the frequency in Figs. (3.2) - (3.5) corresponds to the range from 0 to 500 Hz. The values of $m^{(1)}$ and $\tau^{(1)}$ for which $Z^{(1)}$ is plotted are indicated in the figure captions. The choice $m^{(1)} = 1666$ refers to a hypothetical liquid of high viscosity, $m^{(1)} = 8791$ represents blood at 37°C, and $m^{(1)} = 33088$ corresponds to water at 20°C.

It is seen in Figs. (3.2) and (3.4) that the modulus is a decreasing function of frequency over the range $0 - 500$ Hz. In the low frequencey range, $|Z^{(1)}|$ is observed to fall rapidly with increasing frequency and at all frequencies the more viscous liquid presents a higher impedance modulus although the sensitivity of the quantity to changes in viscosity is not great over the majority of the frequency range. The greatest variation of modulus with viscosity being observed at the lower end of the frequency spectrum. Sensitivity of this quantity to changes

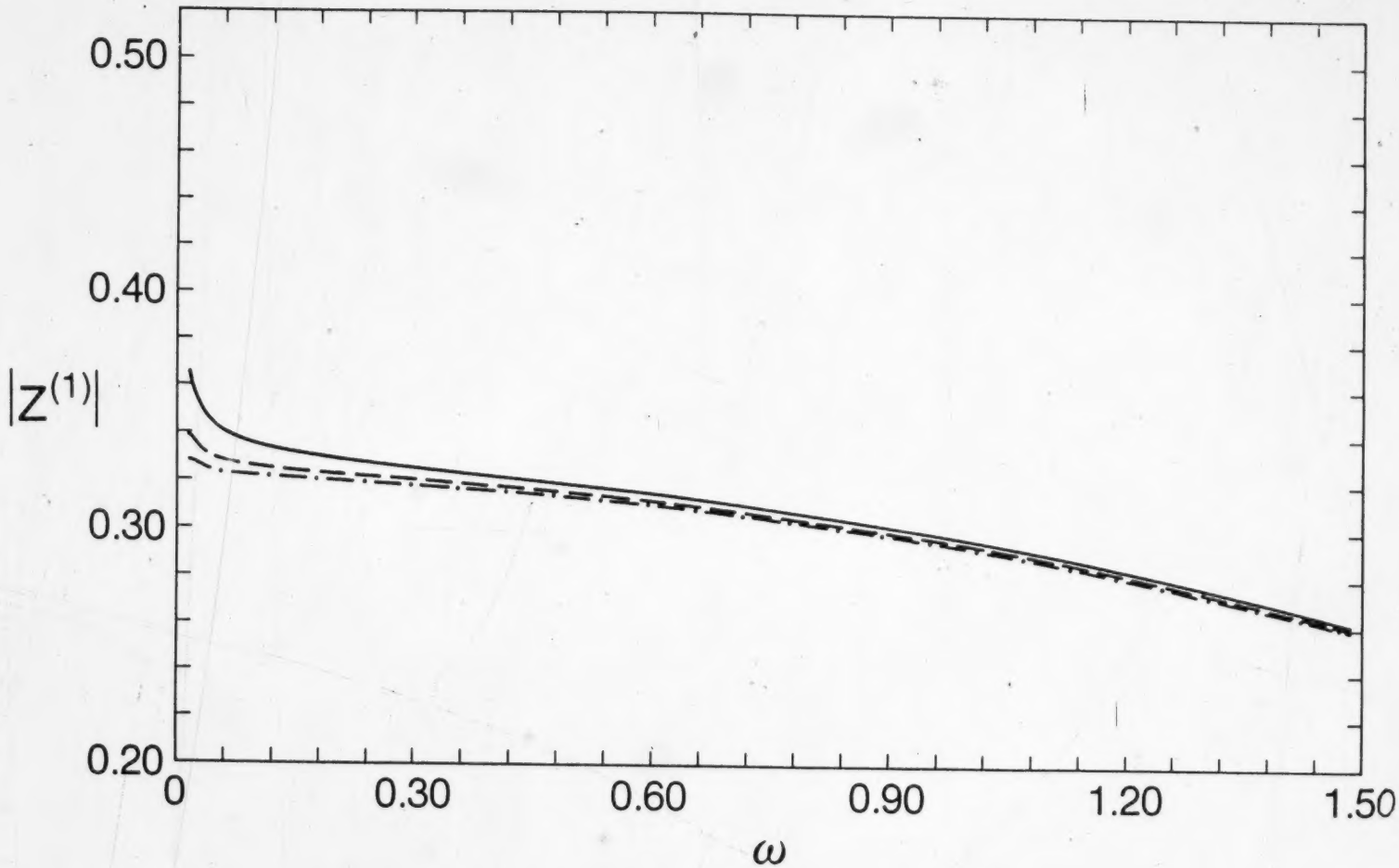

Fig. 3.2 Variation of $|Z^{(1)}|$ with ω for $R^{(1)} = 0.4$cm , $\tau^{(1)} = 0.15$, and $m^{(1)} = 1666$ (—) , 8791 (- - - -) , 33088 (-·-·-·).

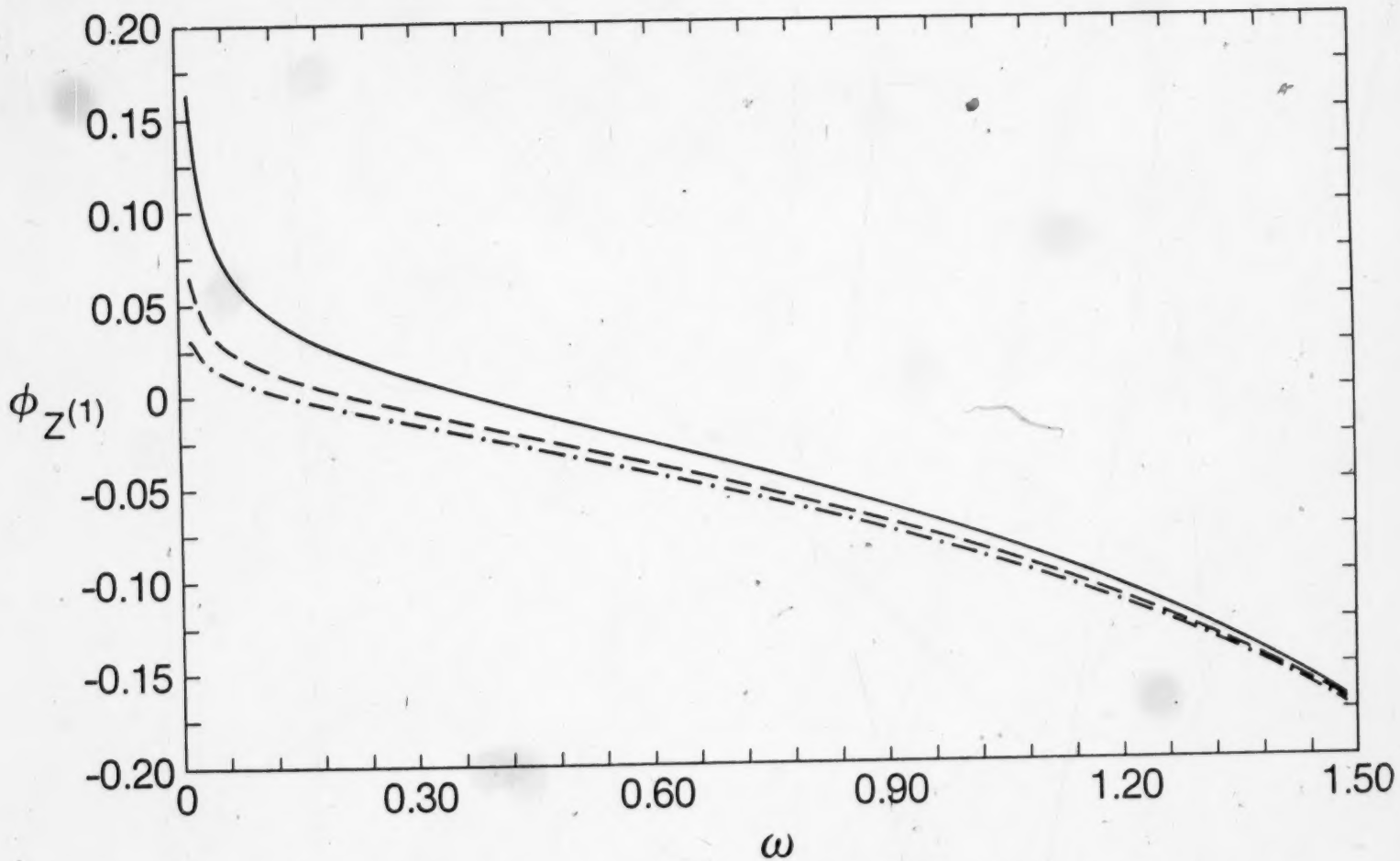

Fig. 3.3 Variation of $\phi_{Z^{(1)}}$ with ω for $R^{(1)} = 0.4$cm , $\tau^{(1)} = 0.15$, and $m^{(1)} = 1666$ (—) , 8791 (- - - -) , 33088 (·····).

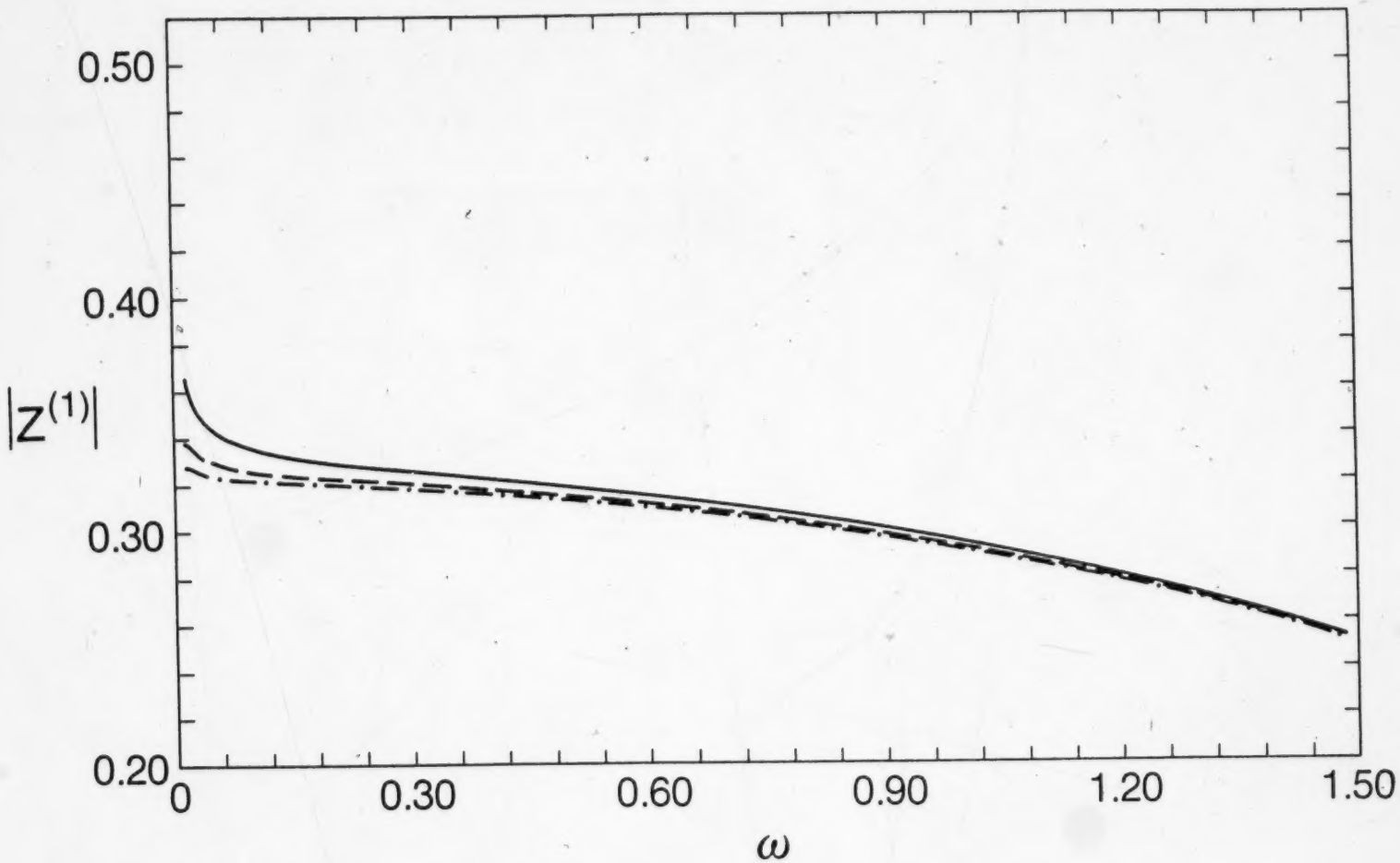

Fig. 3.4 Variation of $|Z^{(1)}|$ with ω for $R^{(1)} = 0.4$cm , $\tau^{(1)} = 0.05$, and $m^{(1)} = 1666$ (—) , 8791 (- - - -) , 33088 (-·-·-·-).

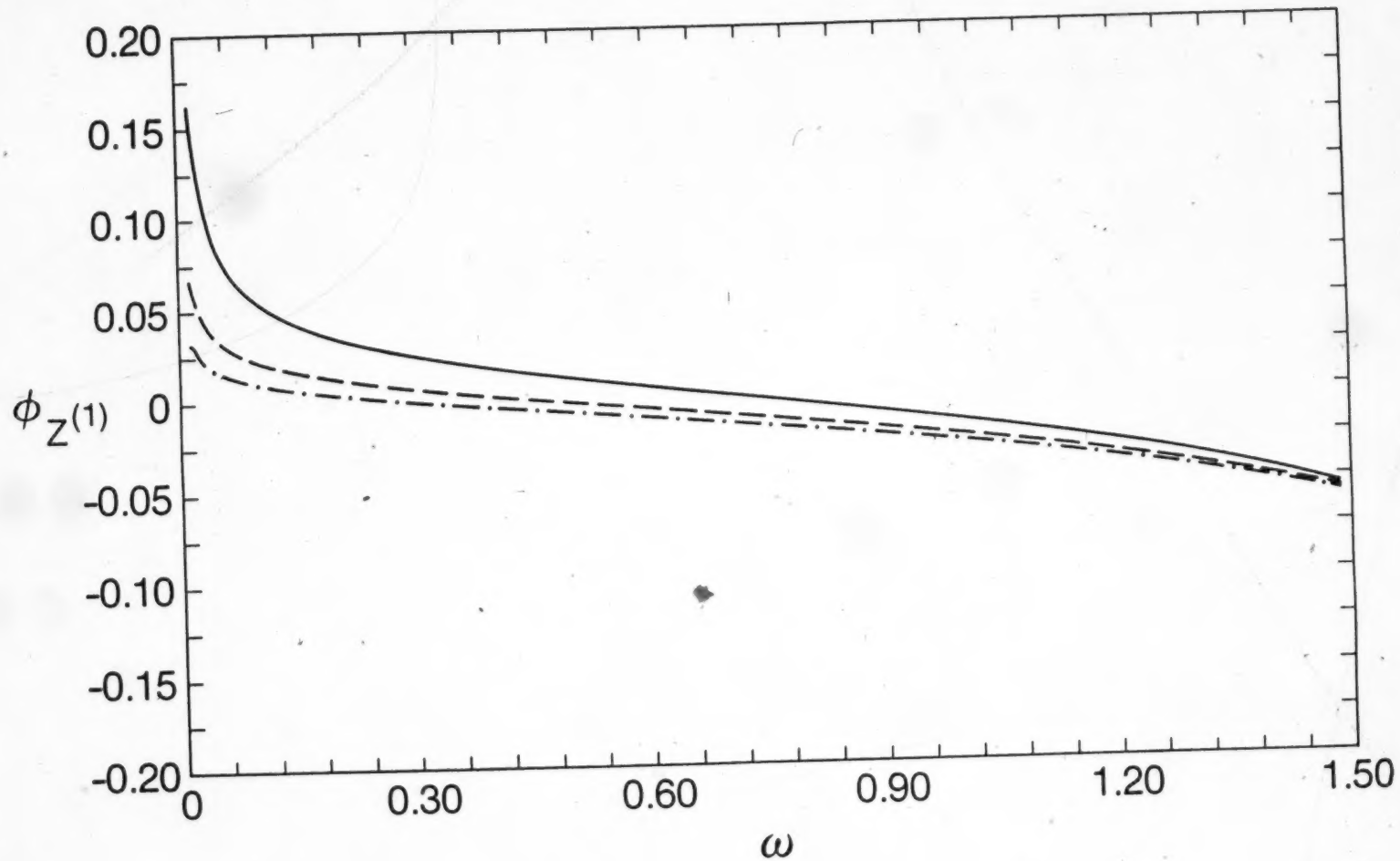

Fig. 3.5 Variation of $\phi_{Z^{(1)}}$ with ω for $R^{(1)} = 0.4$cm , $\tau^{(1)} = 0.05$, and $m^{(1)} = 1666$ (—) , 8791 (- - - -) , 33088 (-·-·-·).

in wall viscoelasticity appears to be even less with the only noticeable changes taking place at the high frequency end. With the phase angle, as shown in Figs. (3.3) and (3.5), the situation is somewhat different in that a greater sensitivity to changes in both viscosity and visocelasticity is observed. In particular it is seen that for higher retardation times, the flow leads the pressure over a greater percentage of the frequency spectrum.

In order to compare the reflection properties of junctions we have introduced the discontinuity coefficient λ_c, reflection coefficient R_c, and transmission coefficient T_{cn}. Because λ_c is a complex valued function of ω, we defined a junction to be "closed" when $|\lambda_c| < 1$ and "open" when $|\lambda_c| > 1$. This agrees with the purely elastic case in that closed junctions produce positive reflections for pressure impulses and open junctions produce negative ones [3]. For definitions in our calculations we have considered a trifurcation ($N = 4$) with $h^{(1)} = h^{(n)}$, $\gamma^{(1)} = \gamma^{(n)}$, $n = 2, 3, 4$, and taken each of the daughter tubes to have the same radius and retardation time. The variations of $|\lambda_c|$ with frequency are illustrated in Figs. (3.6) and (3.7) for closed and open junctions, respectively. Although there are variations with ω and m, $|\lambda_c|$ remains uniformly less than 1 in Fig. (3.6) (closed), and greater than 1 in Fig. (3.7) (open).

For these two cases we have examined the frequency dependence of the effective impedance at A ($x = 0$) in Tube 1. The effective impedance at A, given by Eq. (3.38) or (3.40), is the ratio of oscillatory normal stress in the axial direction to the corresponding oscillatory flow both measured at location A. As

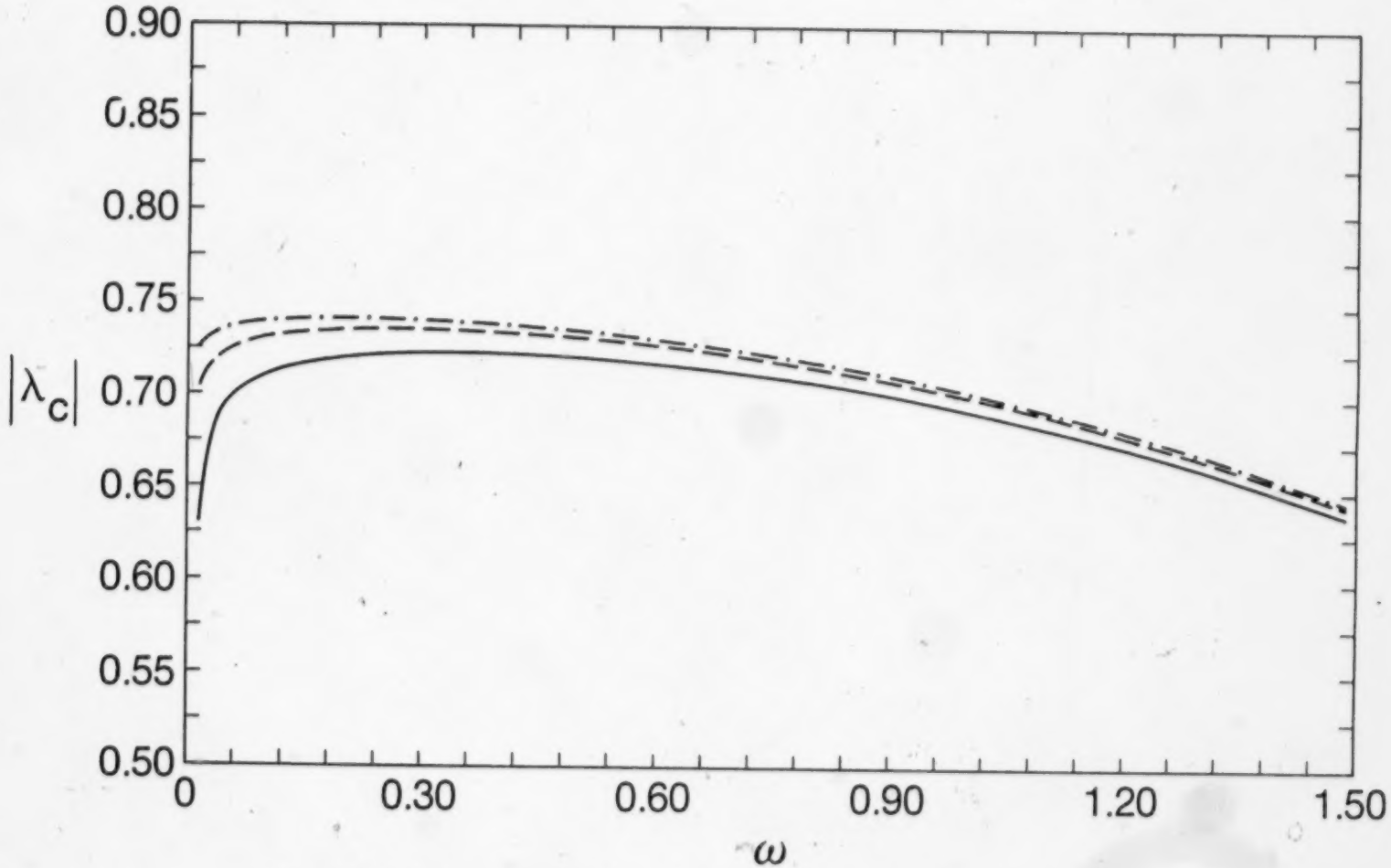

Fig. 3.6 Variation of $|\lambda_c|$ with ω for $R^{(n)}/R^{(1)} = 1/2$, $c_0^{(1)}/c_0^{(n)} = 1$, $\eta^{(1)} = 0.173125$, $\tau^{(1)} = 0.15$, $N = 4$, and $m^{(1)} = 1666$ (—) , 8791 (- - - -) , 33088 (-·-·-·).

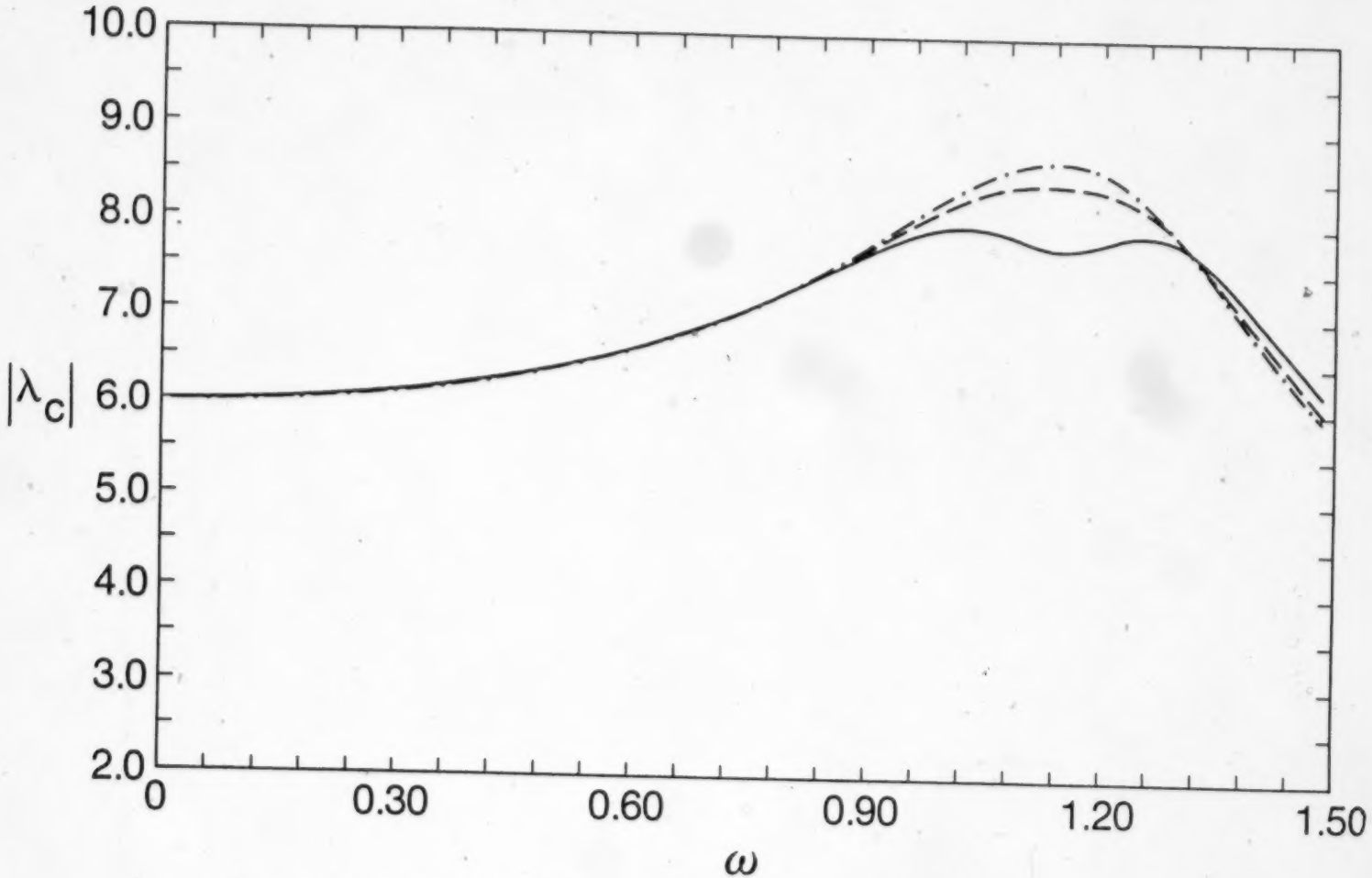

Fig. 3.7 Variation of $|\lambda_c|$ with ω for $R^{(n)}/R^{(1)} = 1$, $c_0^{(1)}/c_0^{(n)} = 2$, $\eta^{(1)} = 0.173125$, $\tau^{(1)} = 0.15$, $N = 4$, and $m^{(1)} = 1666$ (—) , 8791 (- - - -) , 33088 (-·-·-·).

such it is a measure of the resistance to oscillatory flow presented by the system shown in Fig. (3.1). Numerical results for a closed junction are presented in Figs. (3.8) - (3.11) while those for an open junction are given in Figs. (3.12)-(3.15).

It is seen in Fig. (3.8) that the modulus $|Z_{\text{eff}}^{(1)}|$ is high at low frequencies but falls rapidly with increasing frequency to reach the first minimum when the length of Tube 1 is approximately one quarter of a wavelength. It then rises to a maximum when ℓ is one half of a wavelength, falling to the second minimum at three quarters of a wavelength, after which it exhibits succeeding maxima and minima at a whole number of half wavelengths and at an odd number of quarter wavelengths. In Fig. (3.12) it is seen that the modulus $|Z_{\text{eff}}^{(1)}|$ reaches the first maximum when the length of Tube 1 is approximately one quarter of a wavelength, and then decreases to a minimum when ℓ is one half of a wavelength, after which it exhibits succeeding maxima and minima at an odd number of quarter wavelengths and at a whole number of half wavelengths. It shows that the oscillatory behaviour of the modulus $|Z_{\text{eff}}^{(1)}|$ for the closed and open junctions has the phase difference π . On the otherhand, by comparing Figs. (3.8) and (3.12) we see that for a closed junction the minima of the impedance modulus are always greater than those for the open junction. We also observe in these two figures the diminution of maxima and minima of $|Z_{\text{eff}}^{(1)}|$ with increasing viscosity of the fluid. This is especially prominent in the "strongly" open and closed cases which are not included here. Since our system includes dissipative effects, energy supplied at the origin ($x = 0$) is lost in passage along the tube and in addition

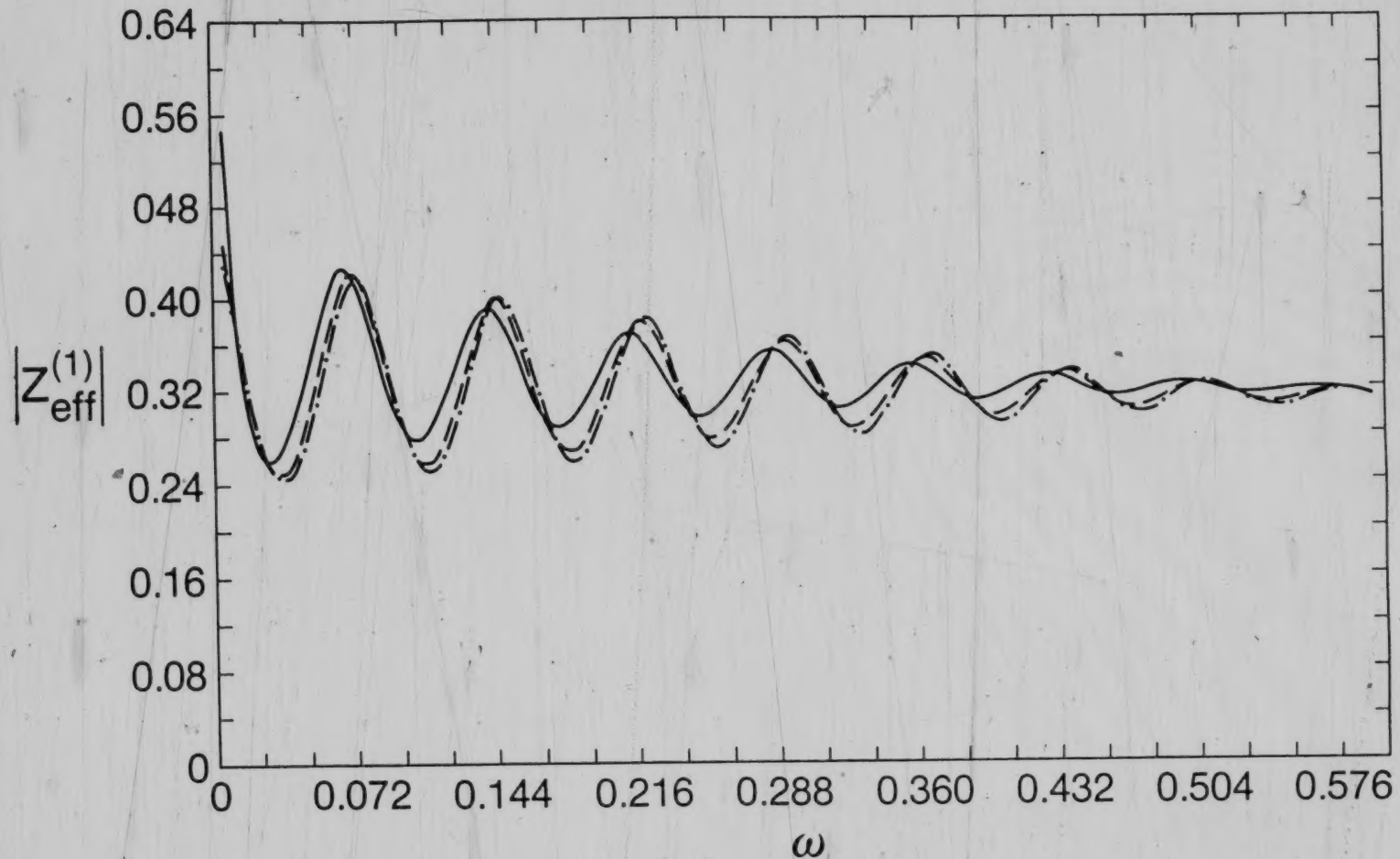

Fig. 3.8 Variation of $|Z_{\text{eff}}^{(1)}|$ with ω for $R^{(n)}/R^{(1)} = 1/2$, $c_0^{(1)}/c_0^{(n)} = 1$,
$\eta^{(1)} = 0.173125$, $\tau^{(1)} = 0.15$, $N = 4$, $\ell = 42$cm, and $m^{(1)} = 1666$ (—) ,
8791 (- - - -) , 33088 (-·-·-·).

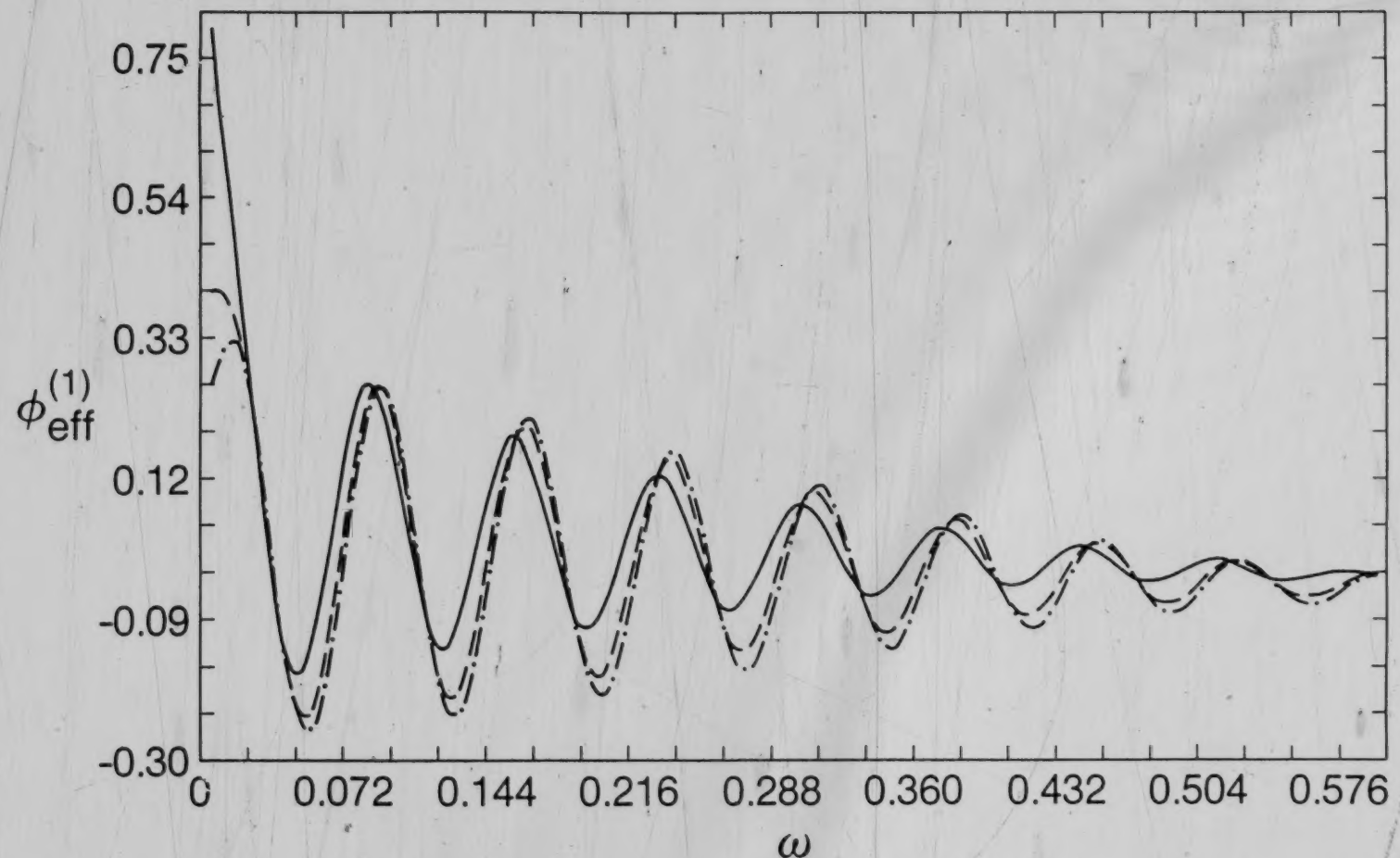

Fig. 3.9 Variation of $\phi_{eff}^{(1)}$ with ω for $R^{(n)}/R^{(1)} = 1/2$, $c_0^{(1)}/c_0^{(n)} = 1$,

$\eta^{(1)} = 0.173125$, $\tau^{(1)} = 0.15$, $N = 4$, $\ell = 42$cm, and

$m^{(1)} = 1666$ (—) , 8791 (- - - -) , 33088 (·····).

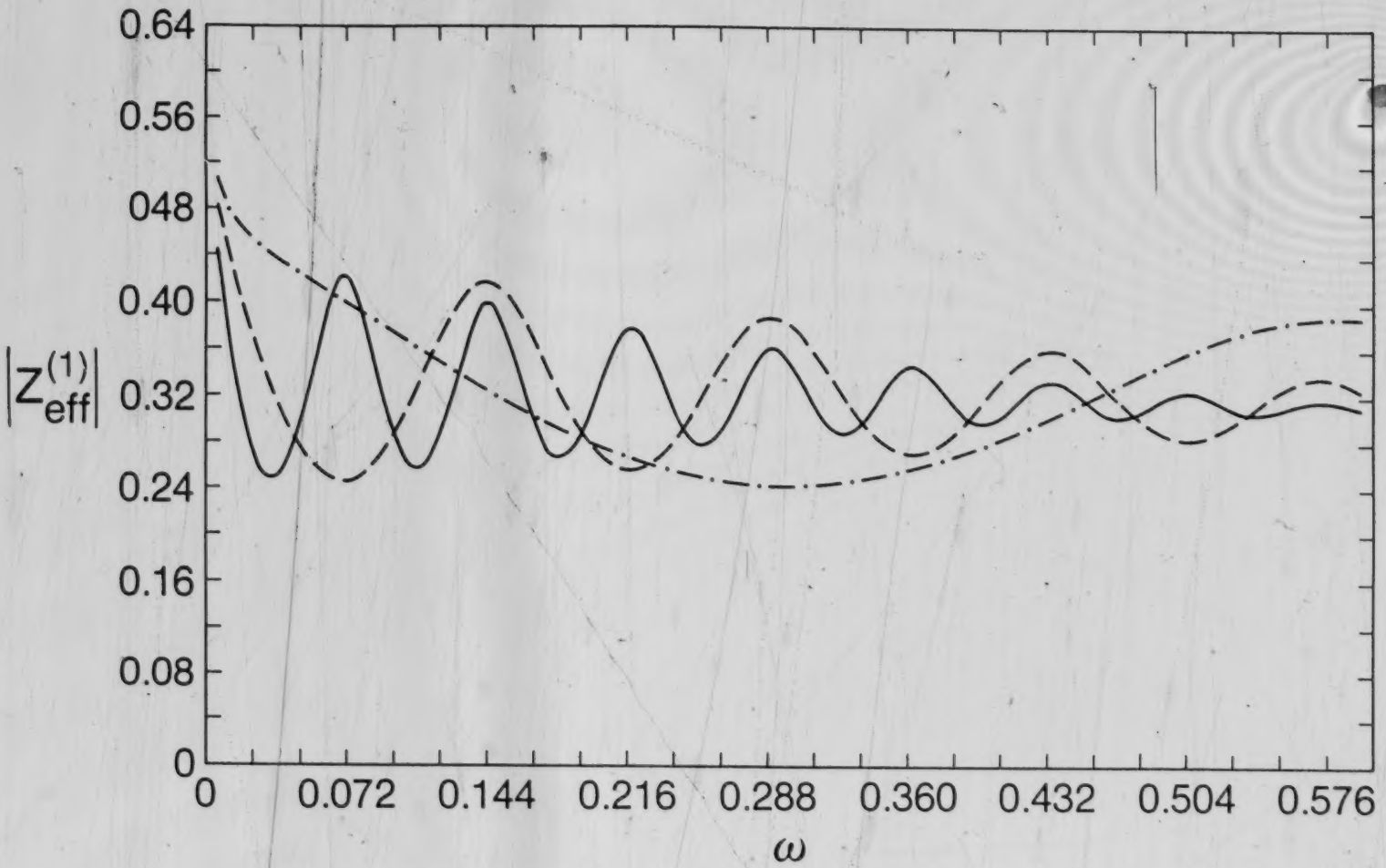

Fig. 3.10 Variation of $|Z_{\text{eff}}^{(1)}|$ with ω for $R^{(n)}/R^{(1)} = 1/2$, $c_0^{(1)}/c_0^{(n)} = 1$,

$\eta^{(1)} = 0.173125$, $\tau^{(1)} = 0.15$, $N = 4$, $m^{(1)} = 8791$, and

$\ell = 42$cm (—) , 21cm (- - - -) , 5cm (-·-·-·).

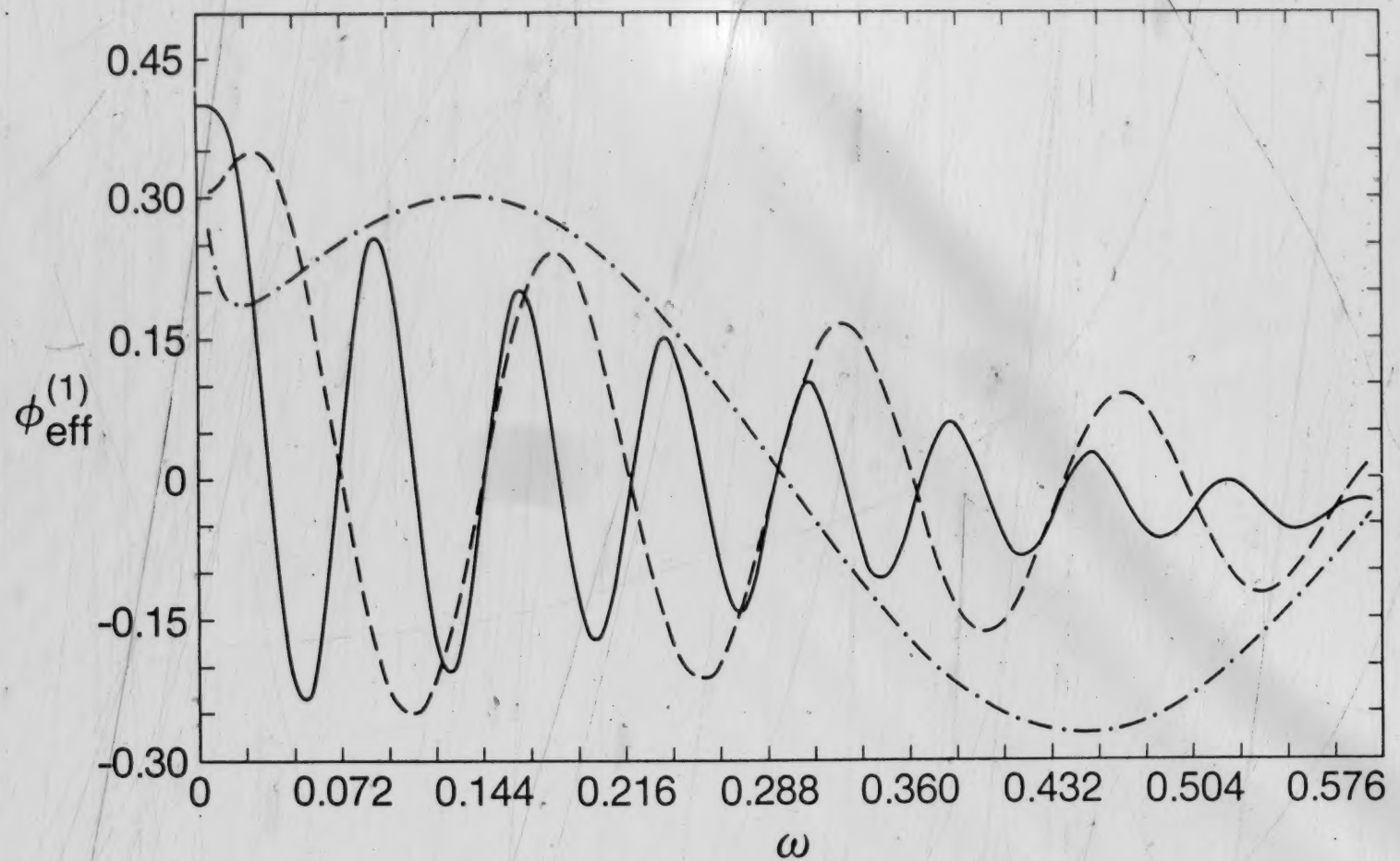

Fig. 3.11 Variation of $\phi_{eff}^{(1)}$ with ω for $R^{(n)}/R^{(1)} = 1/2$, $c_0^{(1)}/c_0^{(n)} = 1$,

$\eta^{(1)} = 0.173125$, $r^{(1)} = 0.15$, $N = 4$, $m^{(1)} = 8791$, and

$\ell = 42$cm (—) , 21cm (-·- - -) , 5cm (-·····).

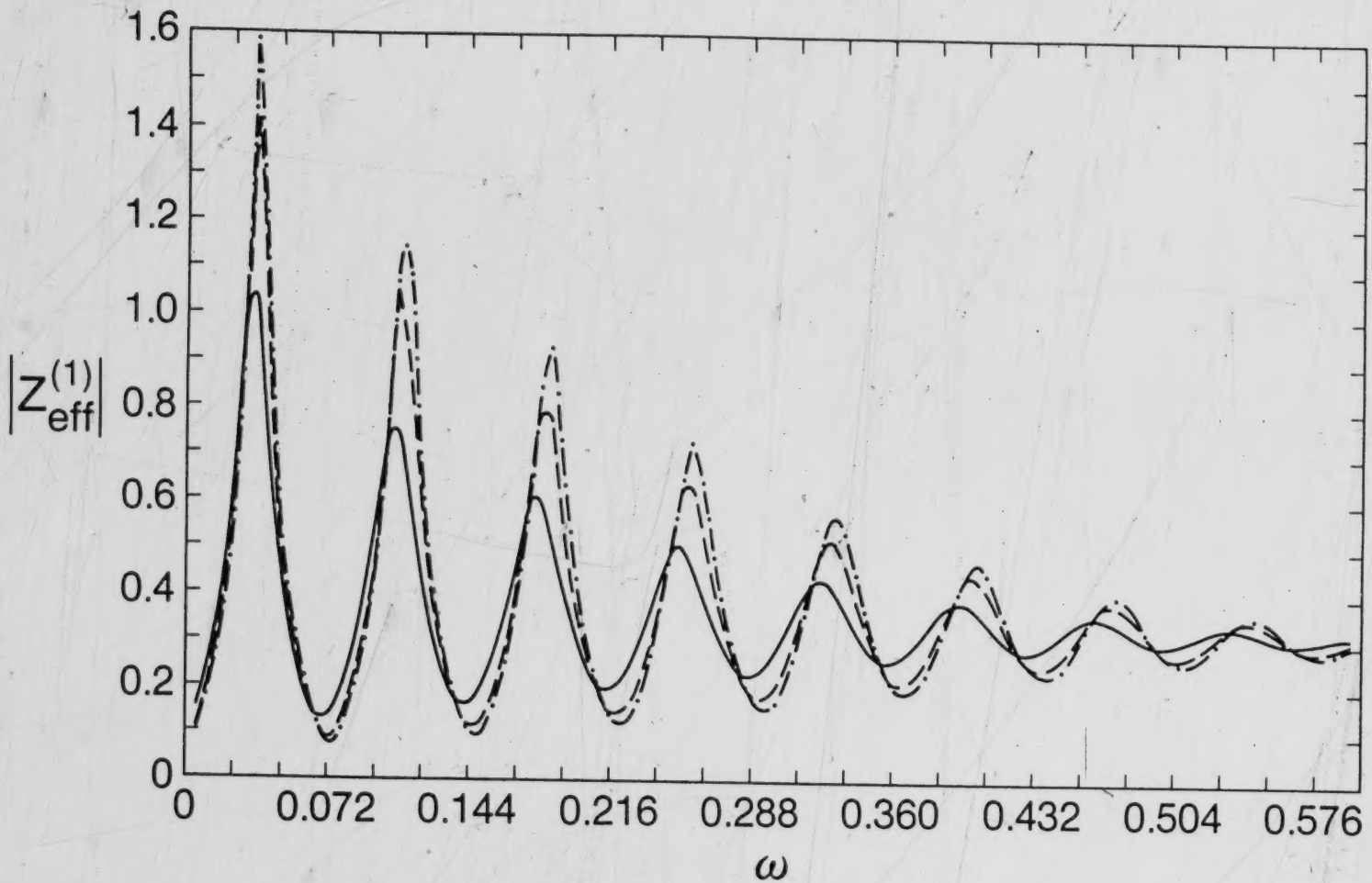

Fig. 3.12 Variation of $|Z_{\text{eff}}^{(1)}|$ with ω for $R^{(n)}/R^{(1)} = 1$, $c_0^{(1)}/c_0^{(n)} = 2$,

$\eta^{(1)} = 0.173125$, $\tau^{(1)} = 0.15$, $N = 4$, $\ell = 42$cm, and

$m^{(1)} = 1666$ (—) 8791 (- - - -) , 33088 (-·-·-·).

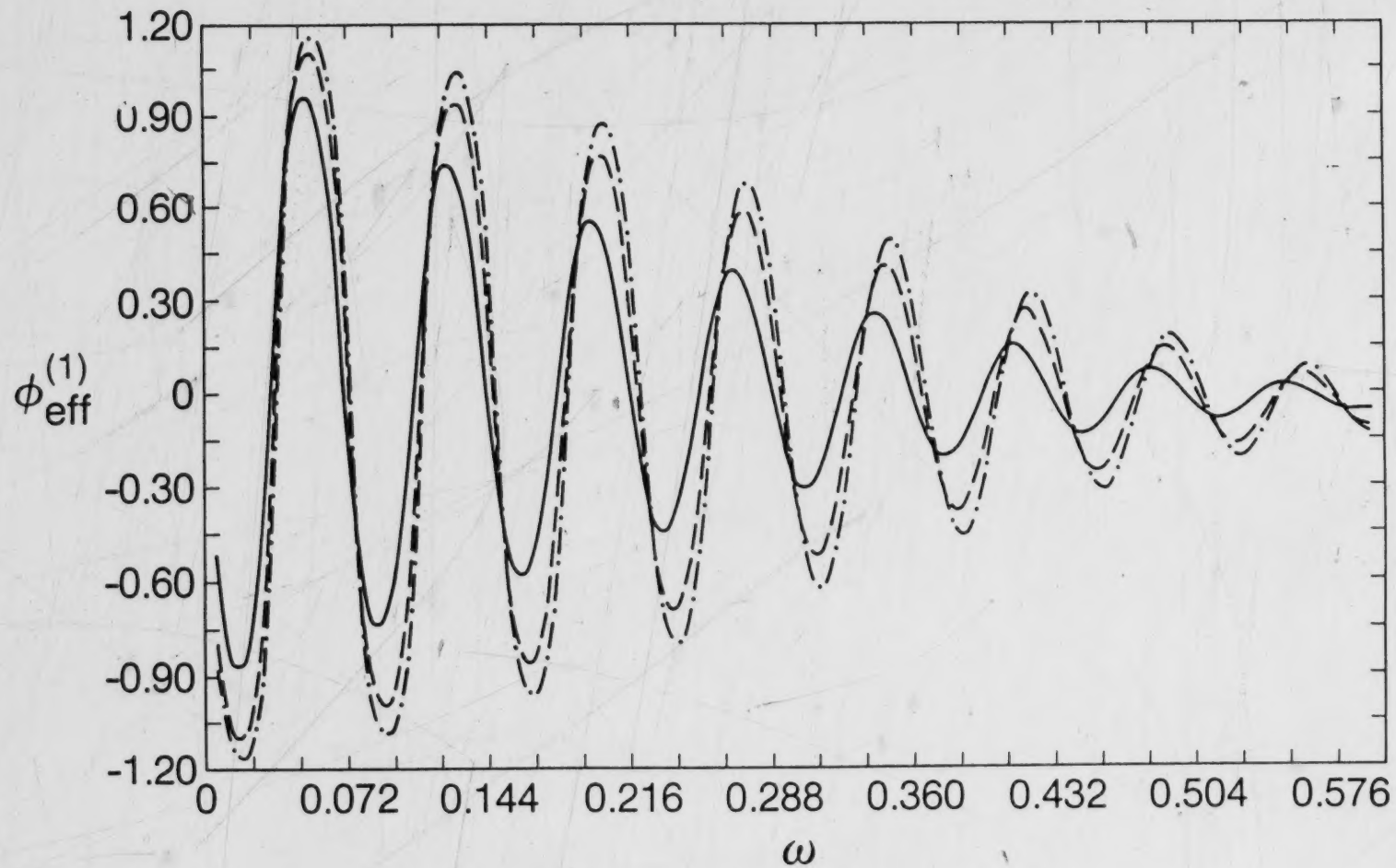

Fig. 3.13 Variation of $\phi_{\text{eff}}^{(1)}$ with ω for $R^{(n)}/R^{(1)} = 1$, $c_0^{(1)}/c_0^{(n)} = 2$,

$\eta^{(1)} = 0.173125$, $\tau^{(1)} = 0.15$, $N = 4$, $\ell = 42$cm, and

$m^{(1)} = 1666$ (—) 8791 (- - - -) , 33088 (-·-·-·).

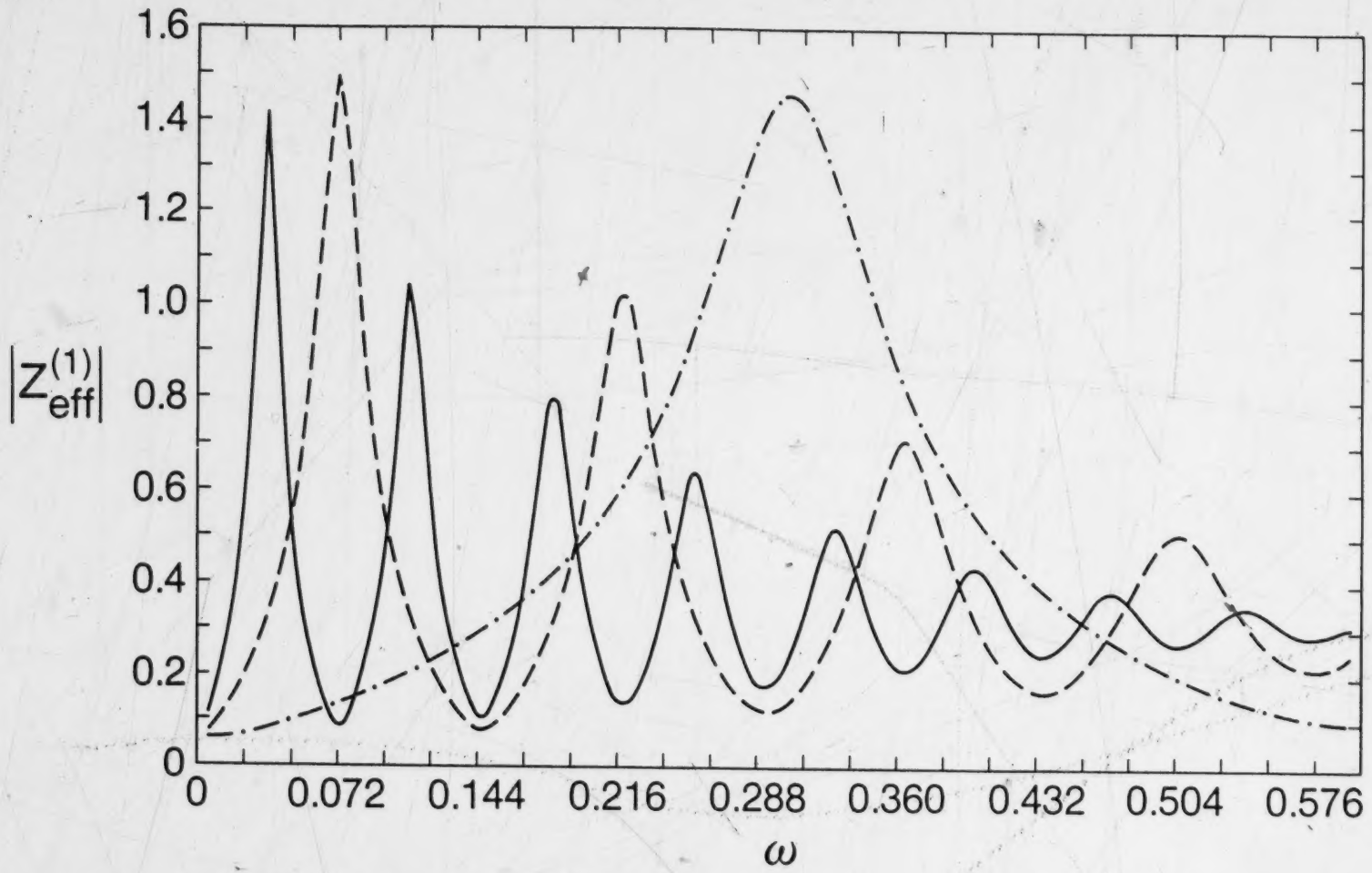

Fig. 3.14 Variation of $|Z_{eff}^{(1)}|$ with ω for $R^{(n)}/R^{(1)} = 1$, $c_0^{(1)}/c_0^{(n)} = 2$,
$\eta^{(1)} = 0.173125$, $\tau^{(1)} = 0.15$, $N = 4$, $m^{(1)} = 8791$, and
$\ell = 42$cm (—) , 21cm (- - - -) , 5cm (-·-·-·).

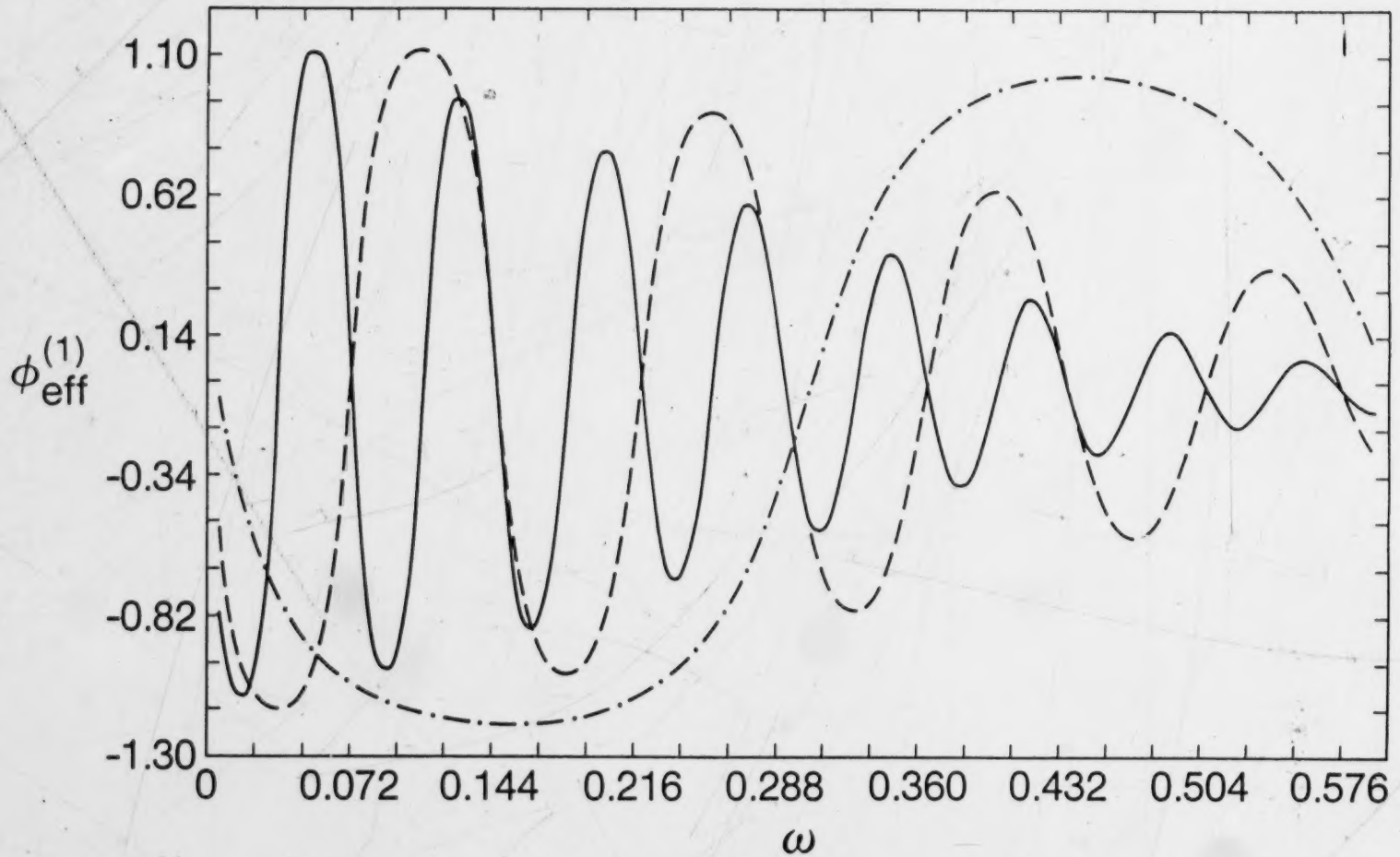

Fig. 3.15 Variation of $\phi_{eff}^{(1)}$ with ω for $R^{(n)}/R^{(1)} = 1$, $c_0^{(1)}/c_0^{(n)} = 2$,

$\eta^{(1)} = 0.173125$, $\tau^{(1)} = 0.15$, $N = 4$, $m^{(1)} = 8791$, and

$\ell = 42$cm (—) , 21cm (- - - -) , 5cm (·····).

may escape into the daughter tubes at the junction ($x = \ell$). These factors imply that the wave from the right is always of smaller modulus than that from the left and can never cancel it so that the development of the true nodes is precluded.

In Figs. (3.9) and (3.13) the phase angles of the effective impedance are plotted as functions of frequency. They exhibit an oscillatory behaviour with amplitude decreasing with increasing viscosity. Again, the open junction case exhibits a greater sensitivity to change in viscosity. Also, in both cases, the phase angle is zero when the modulus is at a minimum.

In Figs.(3.10) and (3.14) we have plotted the modulus of the effective impedance (at $x = 0$) for the closed and open junctions (at $x = \ell$) as a function of frequency while varying the length ℓ of Tube 1. In Fig. (3.10) we see clearly the characteristic initial drop in modulus with frequency and observe that this fall is less rapid with increasing ℓ. The same is true of the data presented in Fig. (3.14) but scaling did not permit us to display the low frequency end. In both of these cases we also observe a decrease in amplitude of the peaks with increasing ℓ.

Figures (3.11) and (3.15) provide the phase angles corresponding to the moduli displayed in Figs. (3.10) and (3.14). The same general remarks as were made before concerning the relation of minima for the moduli to zero values of the phase apply.

CHAPTER IV

Analysis of an Assembly of Tubes

There is overwhelming evidence of pulse wave reflection - and of strong reflection - in the arterial tree of experimental animals and man [20]. These reflections arise from relatively isolated sites of mechanical and/or geometrical mismatch. Fluctuations of impedance modulus and phase are the most precise indicators of this and analysis of impedance patterns provides information on position, intensity, and mechanics of reflections provided results are interpreted in the light of an accurate model of pulse wave propagation and reflection. We now incorporate the previously developed and tested model for pulse propagation in a tube into a representation for the input impedance of a system of branching tubes with multiple reflection sites.

$< A >$ Calculation

Consider an assembly of tubes as depicted in Fig. (4.1) where the properties of each individual tube are based on the experimentally tested shell theory model of Chapter II. It has been suggested [16] that such a parallel architecture may be employed to represent the systemic circulation with the short limb $(B - D)$ representing all arteries supplying the upper body and with the long limb $(B-C)$ representing the descending aorta and lower limb arteries.

The geometric and mechanical parameters of the Tubes 1 and 2 are assumed to be the same and denoted by $R^{(1)}$, $h^{(1)}$, $\gamma^{(1)}$, $G_e^{(1)}$, $\tau^{(1)}$, $\eta^{(1)}$, and $m^{(1)}$. The properties of Tube 0 are the same as those of Tubes 1 and 2 except for $R^{(0)}$

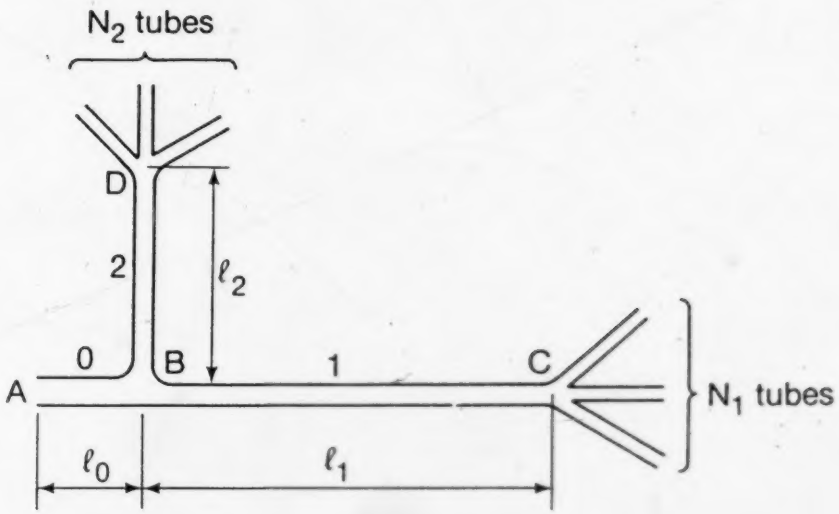

Fig. 4.1 Tube assembly for calculating impedance.

and $c^{(0)}$, where $R^{(0)}$ and $c^{(0)}$ are defined as: $R^{(0)} = 1.29R^{(1)}$, $c_0^{(0)} = 0.78c_0^{(1)}$, and the cross-sectional area ratio at junction B is 1.2 [21]. The parameters associated with the various terminal tubes are denoted by $R^{(n)}$, $h^{(n)}$, $\gamma^{(n)}$, $G_e^{(n)}$, $\tau^{(n)}$, $c_0^{(n)}$, $\eta^{(n)}$, and $m^{(n)}$. According to the prescribed model and the definition of the characteristic impedance $Z^{(n)}$ in Eq. (3.1) we obtain the nondimensional expression of $Z^{(n)}$:

$$Z^{(n)} = \Big\{1 - \frac{2i(k^{(n)})^2}{m^{(1)}\omega}\Big[1 - \frac{F(k^{(n)}R^{(n)}/R^{(1)}}{F(K^{(n)})}\Big]\Big\} \Big\{\pi\Big(\frac{R^{(n)}}{R^{(1)}}\Big)^2 \frac{k^{(n)}}{\omega}\Big[1 - \frac{F(k^{(n)}R^{(n)}/R^{(1)}}{F(K^{(n)})}\Big]\Big\}^{-1}, \tag{4.1}$$

where all variables are nondimensionalized with respect to the parameters of Tube 1 and $n = 0$, for Tube 0, $n = 1$ for Tubes 1 and 2, and $n = 2, \ldots, N_1 + 1$ for the daughter tubes meeting at junction c, and $n = 2, \ldots, N_2 + 1$, for those at D. Also

$$k^{(n)} = \omega \frac{c_0^{(1)}}{c_0^{(1)}} (F_2(K_0^{(1)})\Lambda^{(n)})^{-\frac{1}{2}} \Big[1 + \frac{\omega^2}{2}\Big(\frac{F_3(K_0^{(n)})}{F_2(K_0^{(n)})\Lambda^{(n)}} - \frac{A_1(K_0^{(n)})}{(F_2(K_0^{(n)})\Lambda^{(n)})^2}\Big)\Big(\frac{R^{(n)}c_0^{(1)}}{R^{(1)}c_0^{(n)}}\Big)^2\Big], \tag{4.2}$$

$$\Lambda^{(n)} = 1 - i\omega\tau^{(n)} - \omega^2\Big(\frac{R^{(n)}c_0^{(1)}}{R^{(1)}c_0^{(n)}}\Big)^2\eta^{(n)}, \tag{4.3}$$

$$K^{(n)} = \Big[(k^{(n)})^2\Big(\frac{R^{(n)}}{R^{(1)}}\Big)^2 - im^{(n)}\omega\Big(\frac{R^{(n)}c_0^{(n)}}{R^{(1)}c_0^{(n)}}\Big)\Big]^{1/2}, \tag{4.4}$$

$$K_0^{(n)} = \Big[m^{(n)}\omega\Big(\frac{R^{(n)}c_0^{(1)}}{R^{(1)}c_0^{(n)}}\Big)\Big]^{1/2} e^{-i\pi/4}. \tag{4.5}$$

When reflected waves from the junctions C, D and B are present the transmission properties of the tubes 0, 1 and 2 may be characterized by the effective

impedances. It then follows from Eq. (3.40) that the effective impedance in Tube 1 at position B is

$$Z_{\text{eff}}^{(1)}(B) = \Big[\frac{1 - i\lambda_{cc}\tan(k^{(1)}\ell_1)}{\lambda_{cc} - i\tan(k^{(1)}\ell_1)}\Big] Z^{(1)}, \tag{4.6}$$

wherein λ_{cc} is the discontinuity coefficient of the junction C, defined as

$$\lambda_{cc} = \sum_{n=2}^{N_1+1} \lambda_{cn}, \tag{4.7}$$

where

$$\lambda_{cn} = \Big(\frac{R^{(n)}}{R^{(1)}}\Big)^2 \frac{\beta^{(n)}}{\beta^{(1)}} \Big[\frac{1 - \frac{2ik^{(1)}}{m^{(1)}}\beta^{(1)}}{1 - \frac{2ik^{(n)}}{m^{(1)}}\beta^{(n)}}\Big]. \tag{4.8}$$

By calculations which are essentialy the same as for Tube 1 we may express the effective impedance at B in Tube 2 as

$$Z_{\text{eff}}^{(2)}(B) = \Big[\frac{1 - i\lambda_{CD}\tan(k^{(2)}\ell_2)}{\lambda_{CD} - i\tan(k^{(2)}\ell_2)}\Big] Z^{(2)}, \tag{4.9}$$

where λ_{CD} is the discontinuity coefficient of the junction D, defined as

$$\lambda_{CD} = \sum_{n=2}^{N_2+1} \lambda_{cn}, \tag{4.10}$$

wherein

$$\lambda_{cn} = \Big(\frac{R^{(n)}}{R^{(2)}}\Big)^2 \frac{\beta^{(n)}}{\beta^{(2)}} \Big[\frac{1 - \frac{2ik^{(2)}}{m^{(2)}}\beta^{(2)}}{1 - \frac{2ik^{(n)}}{m^{(2)}}\beta^{(n)}}\Big]. \tag{4.11}$$

The effective impedance at A in Tube 0, called also the input impedance, is then

$$Z_{in} = Z_{\text{eff}}^{(0)}(A) = \Big[\frac{1 - i\lambda_{CB}\tan(k^{(0)}\ell_0)}{\lambda_{CB} - i\tan(k^{(0)}\ell_0)}\Big] Z^{(0)}, \tag{4.12}$$

where λ_{CB} is the discontinuity coefficient of the junction B which can be written in the equivalent form:

$$\lambda_{CB} = \frac{Z^{(0)}}{Z_B}, \tag{4.13}$$

where

$$\frac{1}{Z_B} = \frac{1}{Z_{\text{eff}}^{(1)}(B)} + \frac{1}{Z_{\text{eff}}^{(2)}(B)}. \tag{4.14}$$

Z_{in} of Eq. (4.12) represents the input impedance of the whole system distal to the starting site. It shows clearly that the input impedance is dependent on the frequency, the configuration of discrete reflecting sites, and the mechanical parameters of the system. These dependences will be discussed in the following part.

< B > Analysis of Results

The input impedance Z_{in}, as presented in Eq. (4.12), is a complex valued function of frequency depending upon parameters associated with the architecture (physical dimensions) of the system and the mechanical properties of the fluid and tube wall. In the previous chapter, we have defined two types of junctions: "closed" and "open", which produce positive and negative reflections for pressure impulses, respectively. We now consider the appropriate closed and open cases for the junctions C and D in Fig. (4.1) and plot the dependence of the modulus, $|Z_{in}|$, and the phase angle, ϕ_z, of Z_{in} on the dimensionless frequency ω in Figs. (4.2)-(4.5). Here we have chosen $R^{(1)} = 0.4cm$, $c_0^{(1)} = 833cm/s$, and $\eta^{(1)} = 0.173125$ so that the frequency range in these corresponds to $0 - 20$ Hz. At

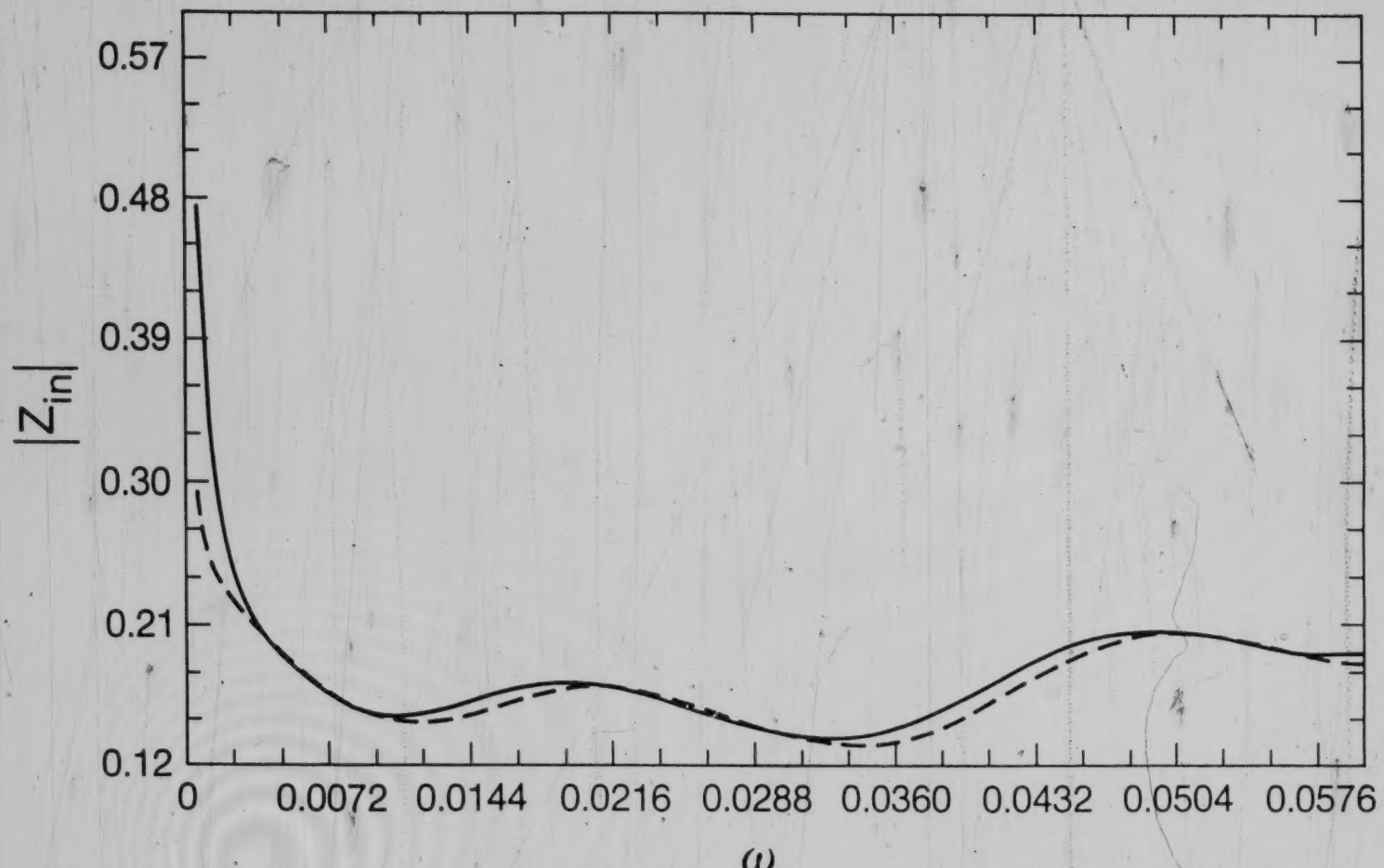

Fig. 4.2 Variation of $|Z_{in}|$ with ω for $\tau^{(1)} = 0.15$, $\ell_0 = 10$cm, $\ell_1 = 120$cm, $\ell_2 = 40$cm, $N_1 = N_2 = 3$, $m^{(1)} = 8791$ (—) , 33088 (- - - -) .

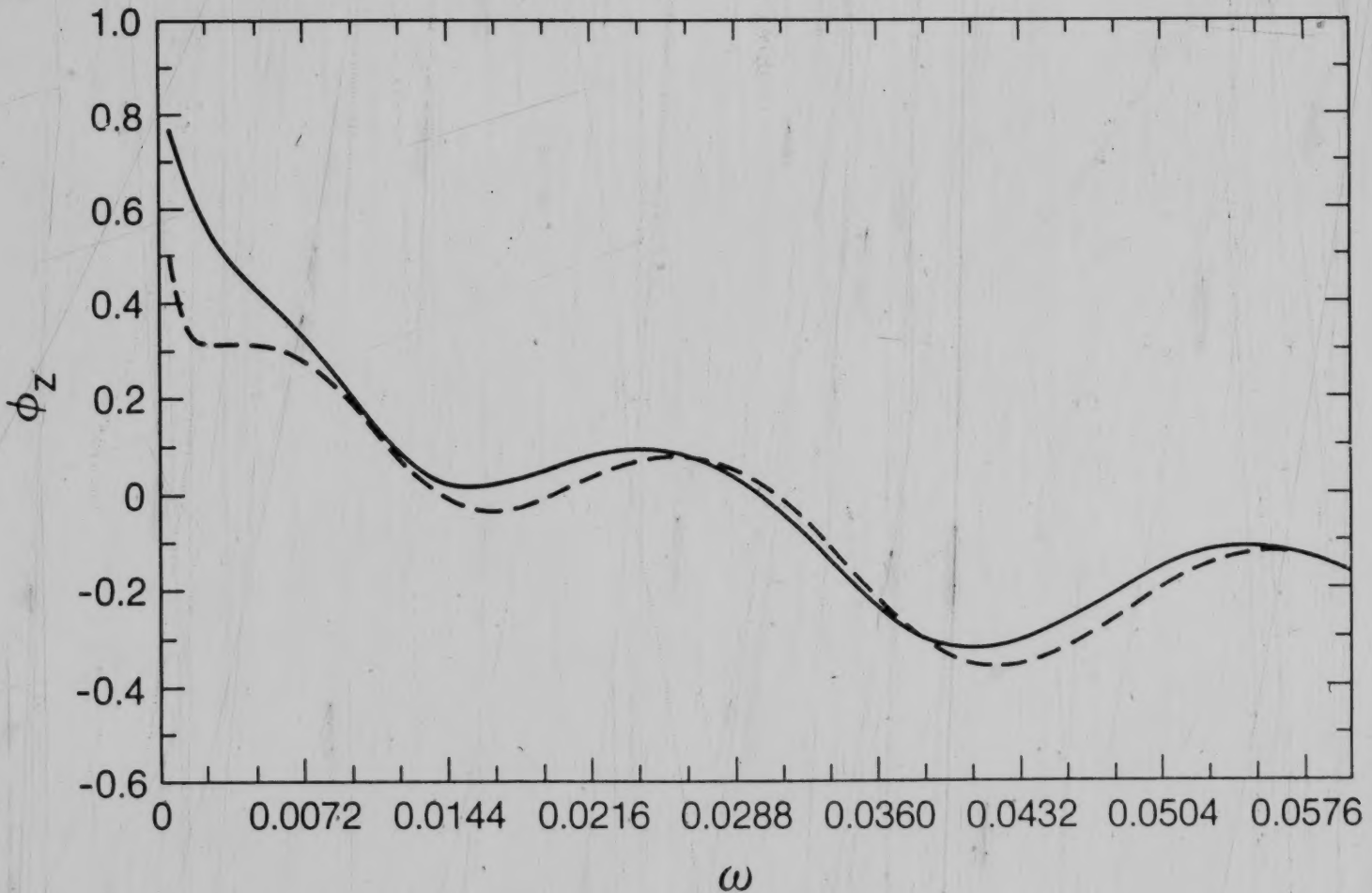

Fig. 4.3 Variation of ϕ_Z with ω for $\tau^{(1)} = 0.15$, $\ell_0 = 10\text{cm}$, $\ell_1 = 120\text{cm}$, $\ell_2 = 40\text{cm}$, $N_1 = N_2 = 3$, $m^{(1)} = 8791$ (——) , 33088 (- - - -) .

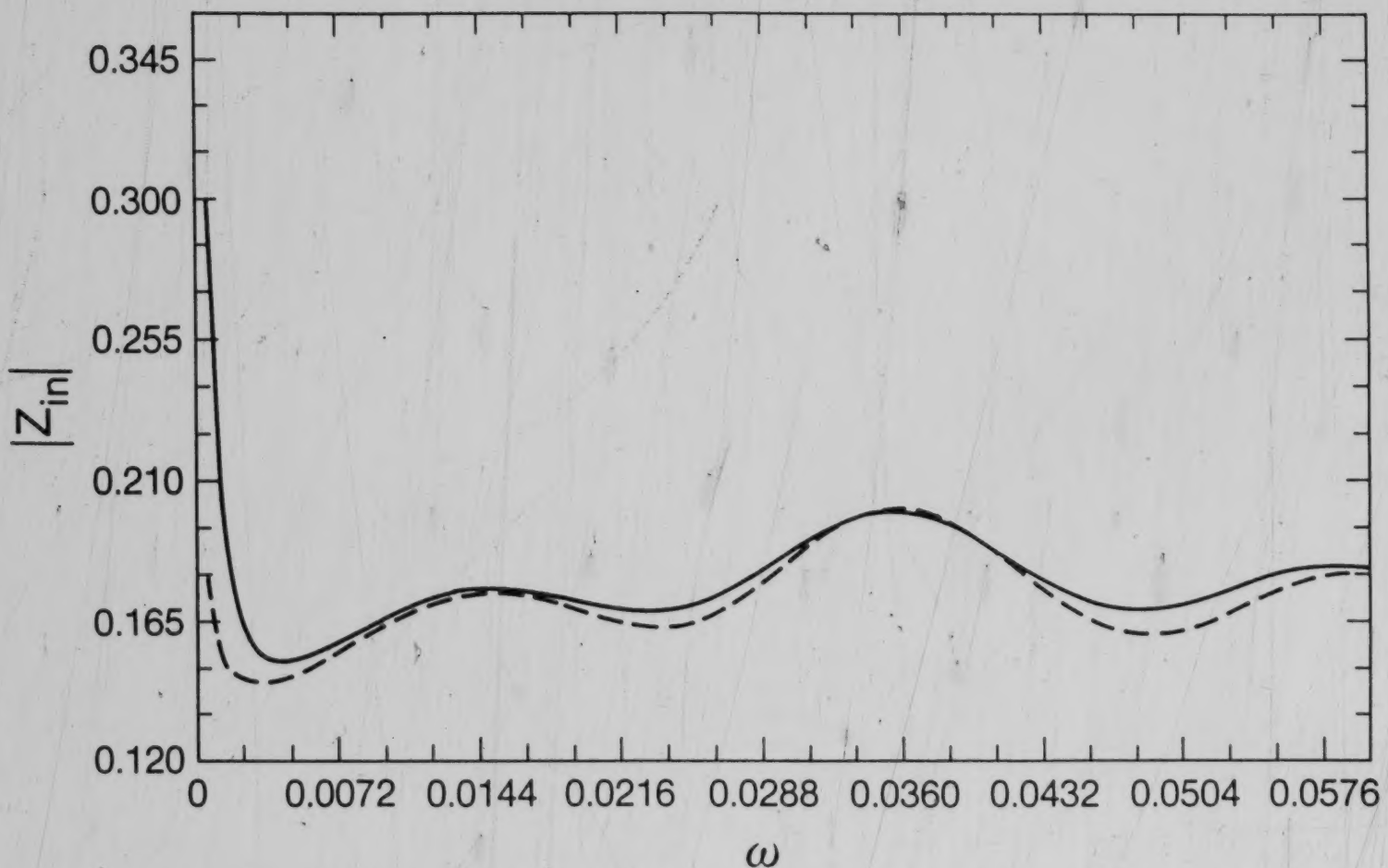

Fig. 4.4 Variation of $|Z_{in}|$ with ω for $\tau^{(1)} = 0.15$, $\ell_0 = 10$cm, $\ell_1 = 120$cm, $\ell_2 = 40$cm, $N_1 = N_2 = 5$, $m^{(1)} = 8791$ (—) , 33088 (- - - -) .

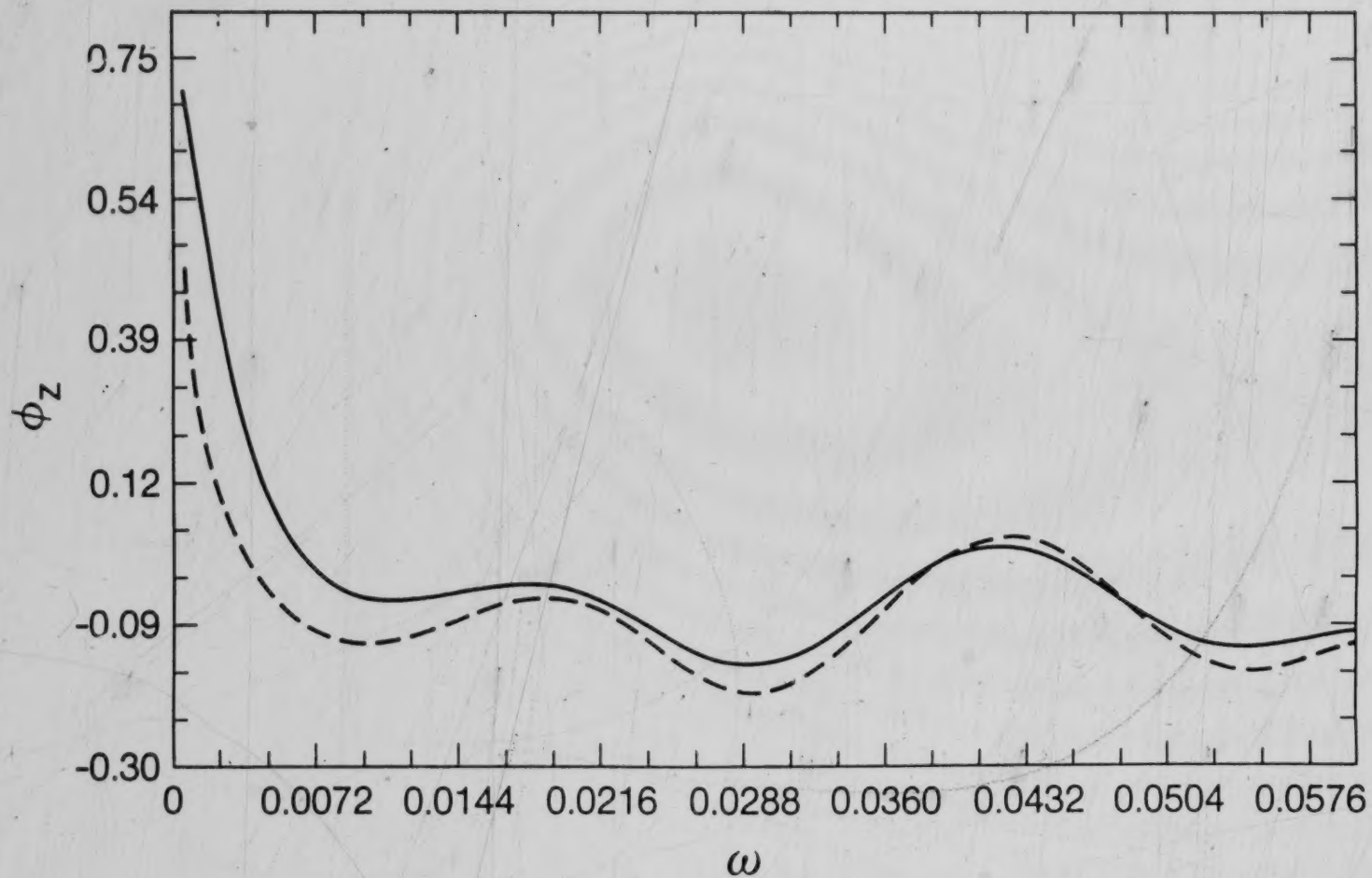

Fig. 4.5 Variation of ϕ_Z with ω for $\tau^{(1)} = 0.15$, $\ell_0 = 10$cm, $\ell_1 = 120$cm, $\ell_2 = 40$cm, $N_1 = N_2 = 5$, $m^{(1)} = 8791$ (—) , 33088 (- - - -) .

junction B, the cross-sectional area ratio, that is, the ratio of the sum of the cross-sectional areas of Tubes 1 and 2 to that of Tube 0, is 1.2. The wave speed in Tube 0, $c_0^{(0)}$, is chosen such that $m^{(0)} = m^{(1)} = m^{(2)}$, and the two values of $m^{(1)}$ that we use, that is, $m^{(1)} = 8791$ and $m^{(1)} = 33088$ correspond to blood at 37°C and water at 20°C, respectively. By this specification we have also that $\tau^{(0)} = \tau^{(1)} = \tau^{(2)}$. For the peripheral junctions at C and D, we assume that each of the daughter tubes has the same radius, wall thickness, density of wall material and retardation time. Thus we have an asymmetrical arrangement. This is analogous to the termination of the arterial system [20].

In Figs. (4.2)-(4.5), when $N_1 = N_2 = 3$, the modulus of the discontinuity coefficient of junction C, $|\lambda_{CC}|$, and the counterpart of junction D, $|\lambda_{CD}|$, are the same, and approximately equal to 0.72 (less than 1) so both junctions are closed; when $N_1 = N_2 = 5$, $|\lambda_{CC}| = |\lambda_{CD}| \approx 1.2$, and both are open.

It is seen in Figs. (4.2) and (4.4) that the modulus $|Z_{in}|$ falls steeply to a minimum at approximately 4 Hz in Fig. (4.2) and approximately 1.5 Hz in Fig. (4.4). The general pattern followed by the modulus of the input impedance over the range depicted in our figures (0-20 Hz) bears a remarkable resemblance to the measured values of aortic impedance modulus in dogs as presented in Fig. 13.13 of McDonald [14]. In fact, the local minima and maxima of $|Z_{in}|$ depicted in our Fig. (4.4) occur at precisely the same frequencies as they do for the experimentally determined plot of [14]. The two distinct minima appearing there at $\omega = 2, 6$ Hz were explained on the basis of the separate reflection effects

from the fore-part and the hind-part of the arterial tree. This broad agreement between theory and observation lends some support for the validity of the model. Upon examination of Figs. (4.3) and (4.5) we observe another phenomenon that has been noted in experimental studies, namely, phase crossovers correspond to maxima and minima of the impedance modulus.

In Figs (4.6) - (4.9) we have examined some of those factors which influence the input impedance. It is seen first from Figs. (4.6) and (4.7) that when ℓ_1 is shortened so that $\ell_1/\ell_2 = 2$ there is a single broad minimum occuring at the frequency of approximately 5 Hz and the phase has only one zero corresponding to this minimum. We here see the influence of the closed junctions at C and D. In their absence the first minimum of $|Z_{in}|$ would occur at a frequency of approximately 20 Hz.

Figures (4.8) and (4.9) when compared to Figs. (4.2) and (4.3) enable us to make some comments concerning the influence of the initial segment of length ℓ_0. Comparing Figs. (4.8) and (4.2), we see that increasing ℓ_0 has the effect of shifting the first minimum to a lower frequency value. The usual correlation between modulus and phase may be observed in Figs. (4.8) and (4.9). Finally, the effect of body size is displayed in Figs. (4.10) and (4.11), where all plots are for $\tau^{(1)} = 0.15$, $m^{(1)} = 8791$ and $N_1 = N_2 = 3$. The shift to the right with decreasing body size is clearly discernible.

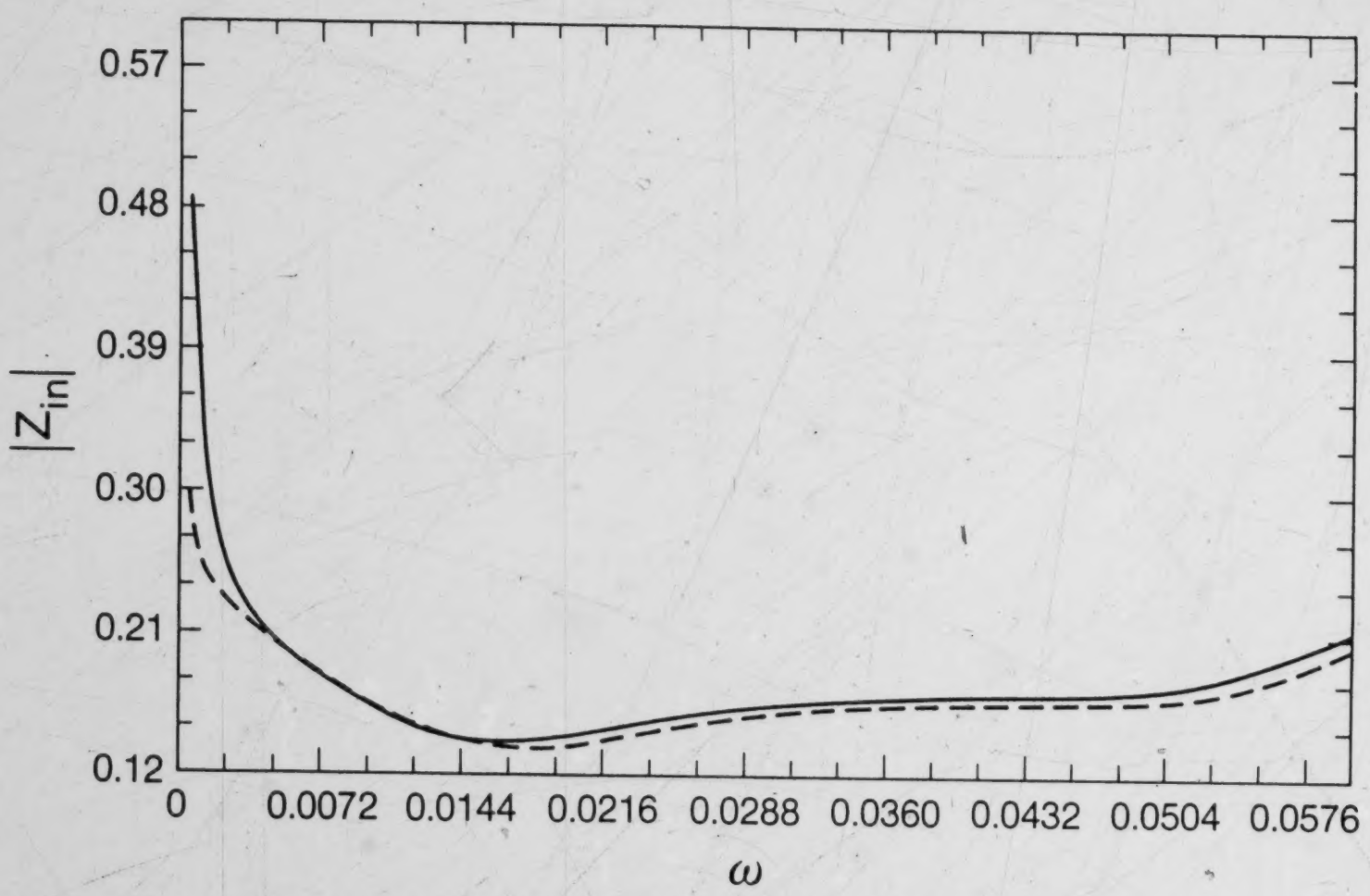

Fig. 4.6 Variation of $|Z_{in}|$ with ω for $\tau^{(1)} = 0.15$, $\ell_0 = 10$cm, $\ell_1 = 80$cm, $\ell_2 = 40$cm, $N_1 = N_2 = 3$, $m^{(1)} = 8791$ (—) , 33088 (- - - -) .

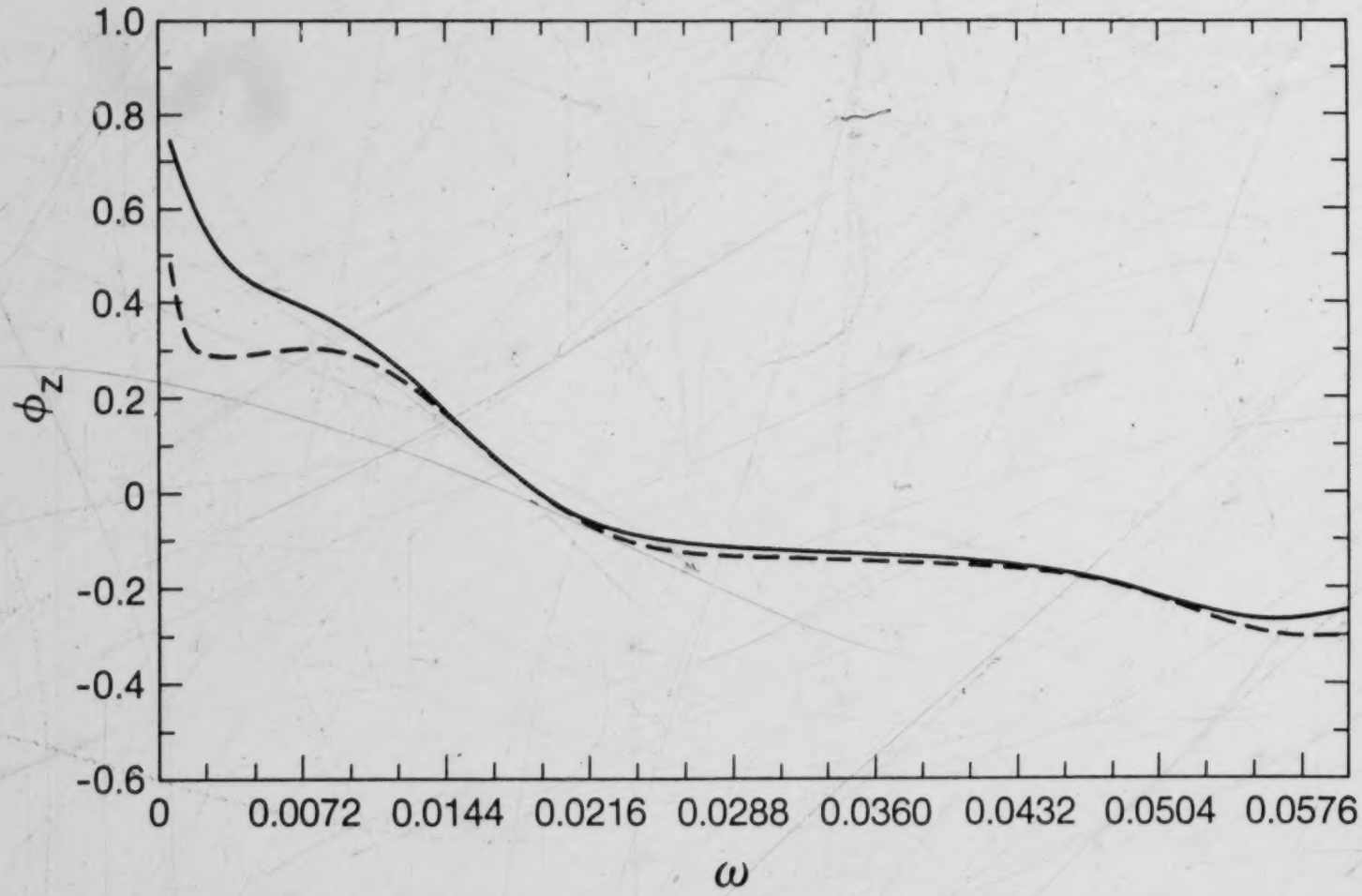

Fig. 4.7 Variation of ϕ_Z with ω for $\tau^{(1)} = 0.15$, $\ell_0 = 10\text{cm}$, $\ell_1 = 80\text{cm}$, $\ell_2 = 40\text{cm}$, $N_1 = N_2 = 3$, $m^{(1)} = 8791$ (—) , 33088 (- - - -) .

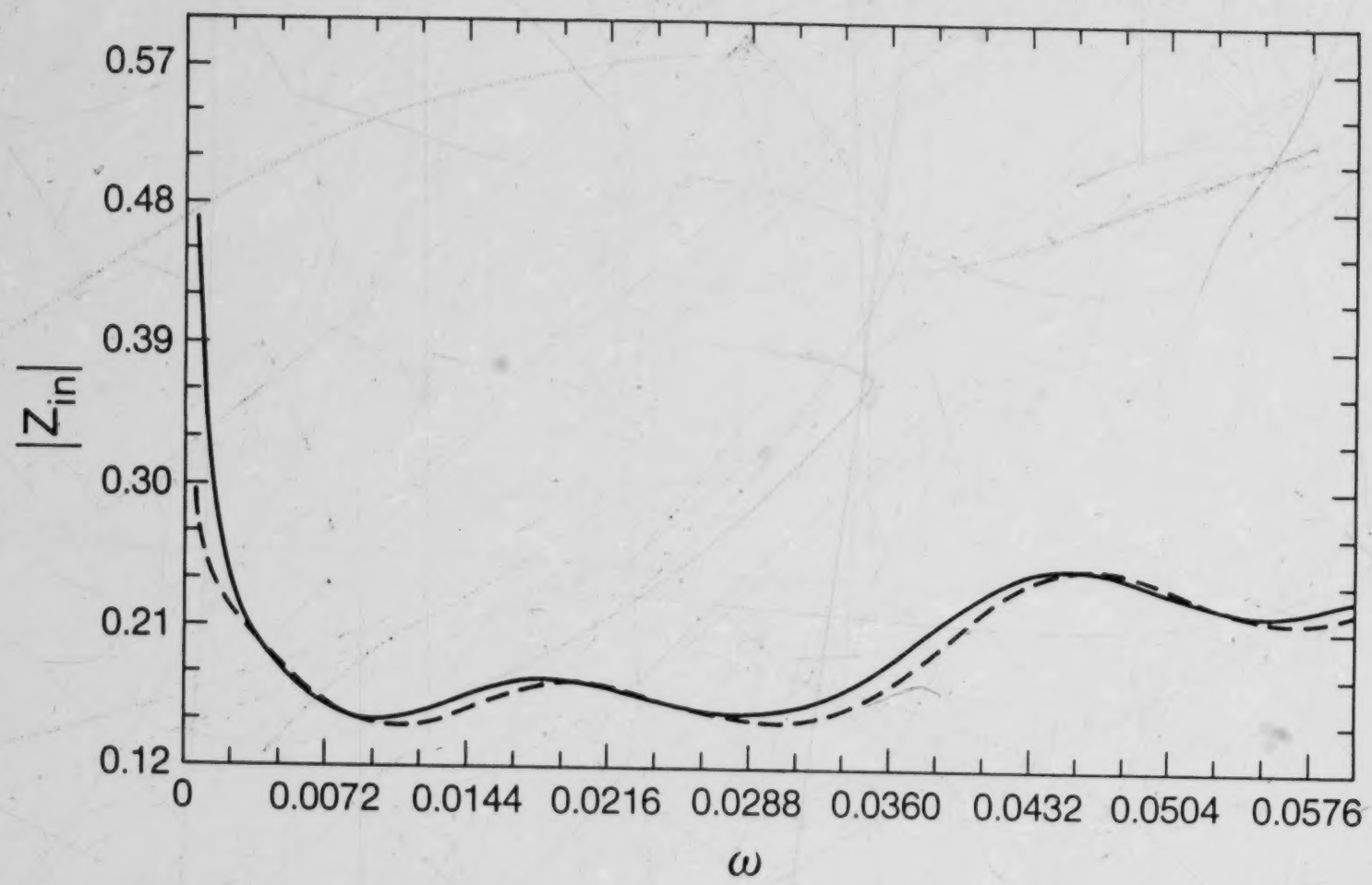

Fig. 4.8 Variation of $|Z_{in}|$ with ω for $\tau^{(1)} = 0.15$, $\ell_0 = 20$cm,

$\ell_1 = 120$cm, $\ell_2 = 40$cm, $N_1 = N_2 = 3$, $m^{(1)} = 8791$ (—) ,

33088 (- - - -) .

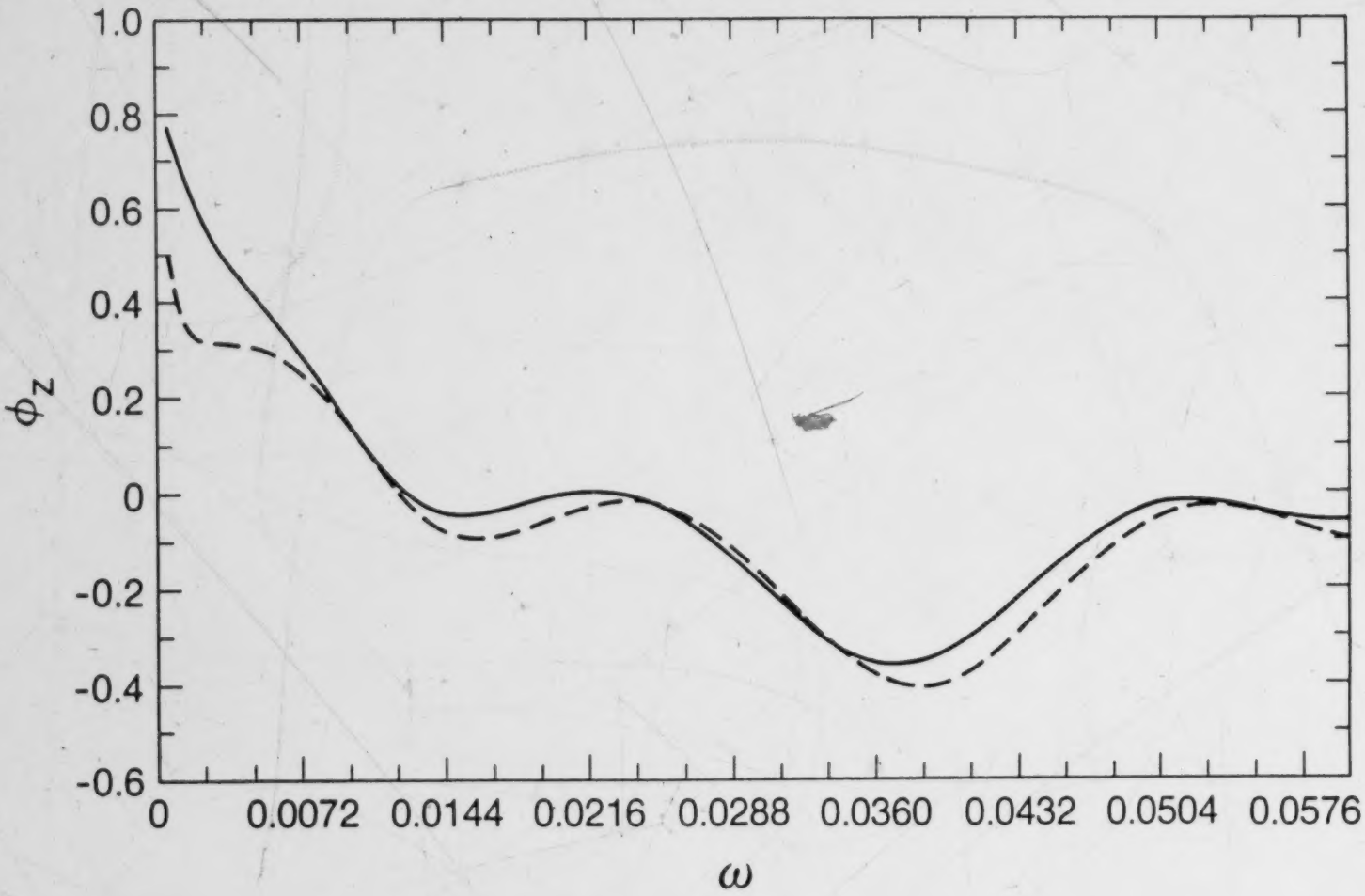

Fig. 4.9 Variation of ϕ_Z with ω for $\tau^{(1)} = 0.15$, $\ell_0 = 20$cm, $\ell_1 = 120$cm, $\ell_2 = 40$cm, $N_1 = N_2 = 3$, $m^{(1)} = 8791$ (—) , 33088 (- - - -) .

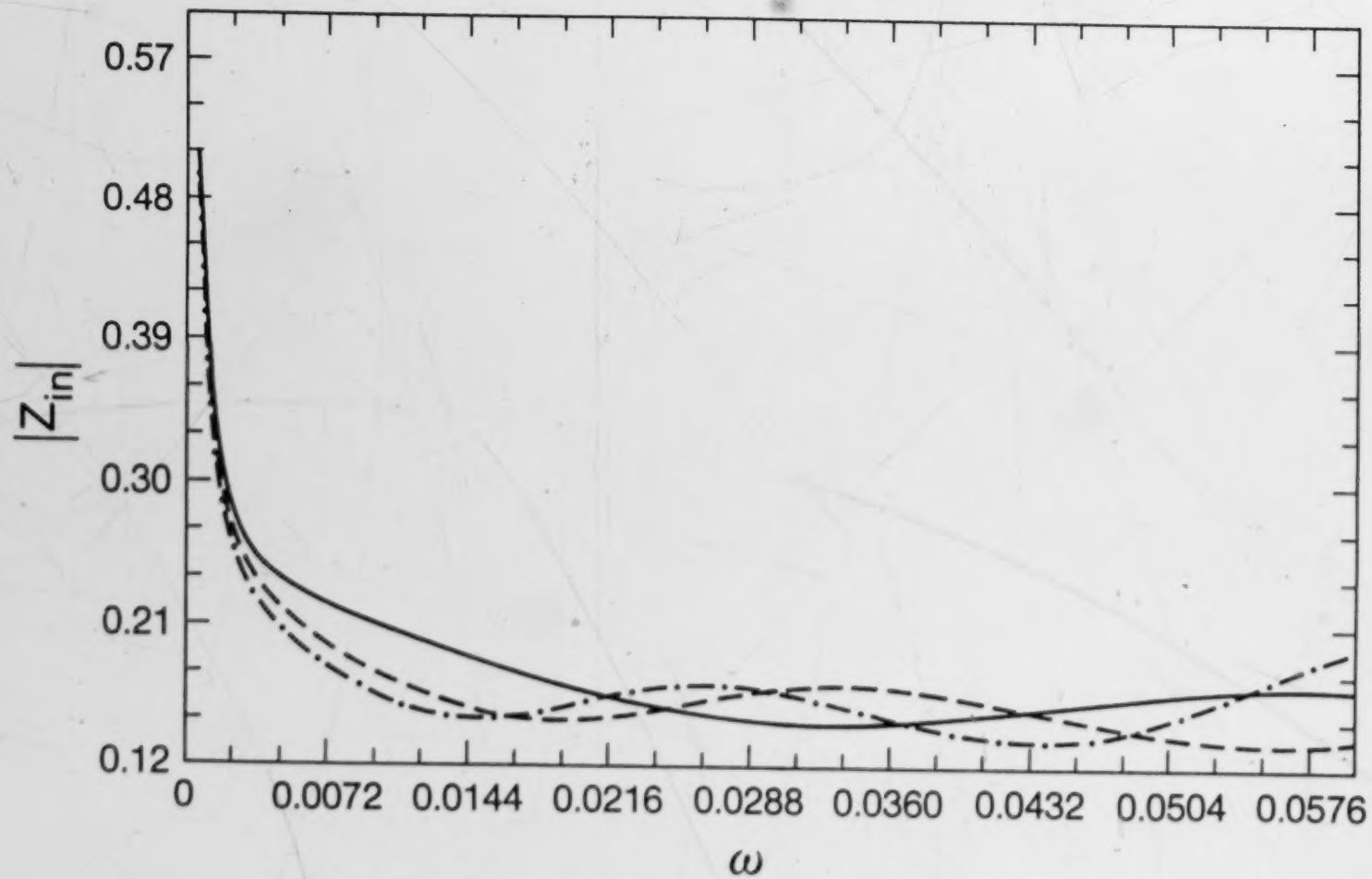

Fig. 4.10 Variation of $|Z_{in}|$ with ω for $\ell_0 : \ell_2 : \ell_1 = 3 : 14 : 42$ (—), $6 : 24 : 72$ (- - - -), $8 : 30 : 90$ (-·-·-).

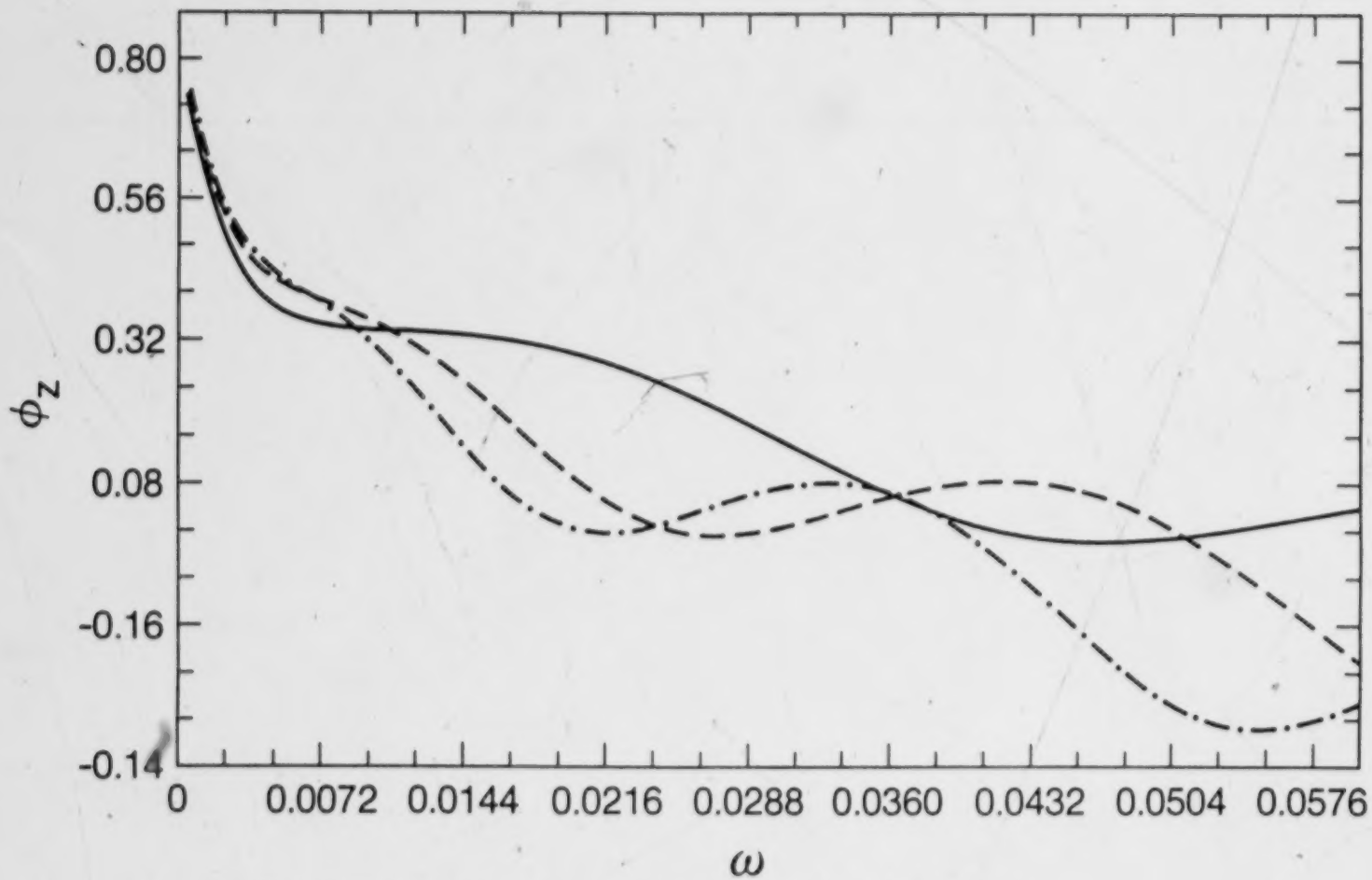

Fig. 4.11 Variation of ϕ_z with ω for $\ell_0 : \ell_2 : \ell_1 = 3{:}14 : 42$ (—), $6 : 24 : 72$ (- - - -), $8 : 30 : 90$ (-·-·-·).

CHAPTER V

Conclusions

In this thesis we have employed an experimentally tested model of wave propagation in fluid filled tubes to study the influence of various factors such as the viscoelasticity of the tube wall, fluid viscosity, and geometry of the system, on both characteristic and effective impedances over a broad frequency spectrum. In contrast to what was found for the reflection coefficients [12] we find that both modulus and phase of the effective impedance are significantly influenced by fluid viscosity. We also found that there was a marked difference in the sensitivity to changes in viscosity of these quantities when calculated for the "closed" and "open" junction with the open displaying the greater sensitivity.

Based on these results, we further studied the frequency dependence of the input impedance for a nearly symmetrical branching system over a frequency range found in dogs. After examining the influence of various factors on the input impedance we have found that the characteristics and positions of reflecting sites have significant effects on both modulus and phase of the input impedance. Compared with the experimental study of dog's ascending aortic impedance [14], [16], [20], our numerical results demonstrate that the patterns of input impedance are attributable to the interacting effects of two separate networks, one being closer to the input than the other, and that there was a marked sensitivity to changes in body size. It is seen that our model gives reasonable qualitative agreement with certain experimental results.

BIBLIOGRAPHY

[1] Newman, D.L., Greenwald, S.E., Denyer, H.T.: Impulse propagation in normal and stenosed vessels. *Cardiov. Res.* 15, 190(1981).

[2] Greenwald, S.E., Newman, D.L.: Impulse propagation through junctions. *Med. & Biol. Eng. & Comput.* 20, 343(1982).

[3] Newman, D.L., Greenwald, S.E., Moodie, T.B.: Reflection from elastic discontinuities. *Med. & Biol. Eng. & Comput.* 21, 697(1983).

[4] Greenwald, S.E., Newman, D.L., Moodie, T.B.: Impulse propagation in rubber tube analogues of arterial stenoses and aneurysms. *Med. & Biol. Eng. & Comput.* 23, 150(1985).

[5] Pedley, T.J.: The Fluid Mechanics of Large Blood Vessels. Cambridge University Press (1980).

[6] Young, T.: Hydraulic investigations subservient to an intended Croonian Lecture on the motion of the blood. *Philos. Trans. Roy. Soc. London* 98, 164-186(1808).

[7] Lighthill, M.J.: Mathematical Biofluiddynamics. Cambridge University Press (1975).

[8] Lighthill, M.J.: Waves in Fluids. Cambridge University Press (1978).

[9] Moodie, T.B., Barclay, D.W., Greenwald, S.E.: Impulse propagation in liquid filled distensible tubes: theory and experiment for intermediate to long wavelengths. *Acta Mech.* 59, 47(1986).

[10] Sawatzky, R.P., Moodie, T.B.: Frequency-dependent reflection from mechanical discontinuities. *Med. & Biol. Eng. & Comput.* 25, 102(1987).

[11] Sawatzky, R.P., Moodie, T.B.: On the propagation of pressure pulses through a viscous fluid contained in a viscoelastic tube. *Q. JL. Mech. Appl. Math.* 41, 33-50(1988).

[12] Sawatzky, R.P., Moodie, T.B.: The role of viscosity in frequency-dependent reflection from discontinuities in liquid-filled tubes. *Med. & Biol. Eng. & Comput.* to appear in 1988.

[13] Newman, D.L., Bowden, N.L.R.: Effect of reflection from an unmatched junction on the abdominal aortic impedance. *Cardiov. Res.* 7, 827(1973).

[14] McDonald, D.A.: Blood Flow in Arteries. Edward Arnold Ltd. (1974).

[15] Fung, Y.C.: Biodynamics: Circulation. Springer-Verlag (1984).

[16] O'Rourke, M.F.: Arterial Function in Health and Disease. Churchill Livingstone (1982)

[17] Whitham, G.B.: Linear and Nonlinear Waves. *New York: Wiley* (1974).

[18] Caro, C.G., Pedley, T.J., Schroter, R.C. and Seed, W.A.: The Mechanics of the Circulation, Oxford University Press (1978).

[19] Gan, R.Z., Moodie, T.B.: Broad-spectrum impedance calculations for arterial models. *Int. J. Engng. Sci.*, to appear in 1988.

[20] O'Rourke, M.F.: Principles of arterial hemodynamics; in: Mechanics of the Circulat (ter Keurs, H.E.D.J., Tyberg, J.V., eds), Martinus Nighoff Publishers (1987).

[21] Taylor, M.G.: The input impedance of an assembly of randomly branching elastic tubes. *Biophys. J.* 6:29(1966).